Supporting Information

Chameleonic dye adapts to various environments shining on macrocycles or peptide and polysaccharide aggregates.

Hang Yin,[1] Frederic Dumur,[2] Yiming Niu,[1] Mehmet M. Ayhan,[2,3] Olivier Grauby,[4] Wei Liu,[1] Chunming Wang,[1] Didier Siri,[2] Roselyne Rosas,[5] Alain Tonetto,[6] Didier Gigmes,[2] Ruibing Wang,[1]* David Bardelang,[2]* Olivier Ouari.[2]*

[1]State Key Laboratory of Quality Research in Chinese Medicine, Institute of Chinese Medical Sciences, University of Macau Avenida da Universidade, Taipa, Macau, China. [2]Aix Marseille Univ, CNRS, ICR, Marseille, France. [3]Department of Chemistry, Gebze Technical University, P.K.:141, 41400 Gebze, Kocaeli, Turkey. [4]Aix Marseille Univ and CINaM, Campus de Luminy, Marseille, France. [5]Aix Marseille Univ, CNRS, Spectropole, FR 1739, Marseille, France. [6]Aix Marseille Univ, Centrale Marseille, CNRS, Fédération Sciences Chimiques Marseille (FR 1739) - PRATIM, 13331 Marseille, France.

* E-mail: rwang@umac.mo (R. W.).
* E-mail: david.bardelang@univ-amu.fr (D. B.).
* E-mail: olivier.ouari@univ-amu.fr (O. O.).

Content

Supplementary Methods.

Chemicals. Methyl iodide and 4-picoline were purchased from Alfa Aesar. 9-methyl-9*H*-carbazole-3-carbaldehyde[1] and 9-octyl-9*H*-carbazole-3-carbaldehyde[2] were synthesized as previously reported in the literature, without modifications and obtained in similar yields. Phe-Phe was from Sigma-Aldrich and Gly-Gly-Gly (DLS control) was from TCI. Fmoc-Leu-Leu was prepared according to the literature and was finely ground into a mortar before use.[3] Cucurbiturils CB[6], CB[7] and CB[8] were prepared according to the literature.[4] Sodium alginate was purchased from Sinopharm Chemical Reagent Co. (Shanghai, China) and Tokyo Chemical Industry Co. (Japan). Amylose from potato and β-Cyclodextrin (99%) were both obtained from Shanghai Yuanye Biotechnology Co., Ltd. All solvents were purchased from Sigma-Aldrich with the best purity available. 18-Crown-6, α-CD, β-CD, DM-β-CD and TM-β-CD were from Sigma-Aldrich. γ-CD was a generous gift from Cyclolab and SBE-β-CD was obtained from Clemens Glaubitz (Institute for Biophysical Chemistry, Goethe University Frankfurt, Germany). The resorcinarene capsule was prepared according to reference 5.[5]

NMR spectroscopy. NMR measurements were recorded on Bruker AVL 300, 400, and 500 spectrometers (^{1}H-NMR 300.13, 400.13, and 500.13 MHz and ^{13}C-NMR 75.46, 100.60, and 125.75 MHz respectively) using D_2O as the solvent (internal reference, 4.70 ppm, watergate sequence (water suppress) used) or DMSO-d_6 (internal reference, 2.50 ppm). Splitting patterns are indicated as follows: s, singlet; d, doublet; t, triplet; m, multiplet.

Mass spectrometry. Mass spectral analyses were carried out using a Q-STAR Elite or a SYNAPT G2 HDMS (Waters) with a TOF analyzer for accurate mass measurements at the Aix Marseille Université Mass Spectrum Facility, Spectropole Saint Jérôme Marseille.

Elemental analysis. Elemental analyses were performed using a Flash EA analyser, 1112 series Thermo Finnigan driven by the Eager 300 software (oven temperature: 970°C, gas: helium, flow rate: 140 mL/min, detector: catharometer).

UV and fluorescence (solvent study and Φ after CB[*n*] binding). Absolute fluorescence quantum yields (solvents studies and after CB[*n*] binding) were measured by a Hamamatsu Photonics Quantaurus QY at room temperature. Absorption and emission spectra were recorded with a UV MC2 spectrophotometer from the SAFAS Monaco Society and a Photon Technology International spectrofluorimeter.

UV and fluorescence (stoichiometry and binding studies). The UV-visible spectroscopic binding studies were performed using a HACH DR6000 UV-visible spectrometer with a 1.0 cm path length quartz cell. The fluorescence spectroscopic binding studies were performed using a Lumina™ fluorescence spectrophotometer from Thermo Scientific with a 1.0 cm path length quartz cell. All binding affinities were calculated by using Origin 8.0.

Continuous variation titrations: To prepare solutions for continuous variation titrations (Job plots), solutions with a total concentration of 0.04 mM of LFD-**01** and CB[*n*] (*n*=6, 7, 8) were prepared in Milli-Q water. Among these solutions, the ratio of CB[*n*]/([LFD-**01**]+CB[*n*]) was varied from 0 to 1.0 by steps of 0.1.

UV/Fluo titrations: To prepare the UV-visible/fluorescence spectroscopic titrations, solution of LFD-**01** (0.02 mM) was prepared in Milli-Q water. The solution was then titrated with various volumes of solution containing the same concentration of LFD-**01** and 6.0 equivalent CB[*n*] (*n*=6,7,8).

UV and fluorescence (dipeptide study). The UV and fluorescence spectra involving the dipeptide were performed on an Infinite M200 spectrofluorometer from Tecan. Kinetic cycles were programmed over period comprised between 1 and 2 hours. Excitation was done at 262 nm for experiments involving Fmoc-Leu-Leu (at 0.1, 1, 4 and 36 mM) to probe Fmoc-Leu-Leu assembly by UV and PL and for the energy transfer experiments (FRET, see Fig. 7b) using LFD-**01** at 0.1 and 1 mM final concentrations. An excitation of 420 nm was used for the kinetics of self-assembly using Fmoc-Leu-Leu (4, 12 and 36 mM) as monitored by the fluorescence of LFD-**01** (0.1 mM). Samples of LFD-**01** at 0.105 or 1.05 mM were prepared in water (ultrasound 120 seconds: ultrasound cleaner bath Bandelin Sonorex, frequency 35 kHz, and power 215/860 W) to get 0.1 and 1 mM final concentrations when

required. A stock solution of NaOH (1M) was prepared to get 36 mM concentration after dilutions. As the self-assembling process starts right after the dissolution of Fmoc-Leu-Leu by the addition of NaOH, we took care of minimizing the time of mixing and sample introduction to avoid losing information. The minimum time was set to 40 seconds before the first fluorescence measurement could be obtained (see Fig. S45). For the FRET measurements, several concentrations were assessed but the one allowing the most efficient energy transfer was 36 mM Fmoc-Leu-Leu and 1 mM LFD-**01**. Other combinations using Fmoc-Leu-Leu at 0.1, 1, 4, and 36 mM and LFD-**01** at 0.1 and 1 mM ended up with some cases where energy transfer occurred but not as clearly as for the aforementioned conditions. The gain was fixed to 65 for experiments of Fig. 7a for the sake of comparison, at 83 for the FRET experiments reported in Fig. 7b and at 81 for the spectra of Supplementary Fig. 45.

UV and fluorescence (alginate study). LFD-**01** was suspended in distilled water (2.5 mM stock solution) using ultrasound for 10 minutes just before dilutions (swept ultrasound cleaner bath SB-300DTY, frequency 25 kHz, and power 0.35 W/cm^2). A series of polysaccharide samples (1%, m/m, 60°C for dissolution) containing 50 μM LFD-**01** were prepared separately in 1.5 mL microcentrifuge tubes (1st series of measurements). Then, this solution was injected (1/5, $v_{alginate}/v_{Ca2+}$) in a $CaCl_2$ solution (5%, m/m) resulting in immediate gelation (2nd series of measurements on the gel). The fluorescence spectra of 50 μM LFD-**01** in the presence of alginate were performed with Thermo Lumina fluorescence spectrometer. The emission wavelengths were monitored from 450 nm to 750 nm at an excitation wavelength of 415 nm. Slits were set to 5 nm bandpass both in excitation and emission, the scanning speed was set at 300 nm/min and the PMT voltage was 450 V. UV-visible absorption spectra were acquired with a DR6000 UV-Vis Spectrophotometer (Hach).

UV and fluorescence (amylose study). 10 mg of amylose was dispersed into 5 mL milliQ water to form an amylose aqueous suspension (2%, w/v). Similarly, a 2% β-Cyclodextrin aqueous solution (w/v) was prepared. 100 μL of LFD-**01** stock suspension (2.5 mM, 10 minutes ultrasound) was separately added in the amylose suspensions/solutions or β-cyclodextrin solutions with constant stirring. The fluorescence spectra of 50 μM LFD-**01** in polysaccharide solutions were recorded with a Thermo Lumina fluorescence spectrometer. PL spectra were acquired at 0h, 0.5h, 1h and 5h of incubation time (before each measurement, the mixtures were repeatedly pipetted up and down for homogenization). The emission wavelengths were monitored from 450 nm to 750 nm at an excitation wavelength of 415 nm. Slits were set to 5 nm bandpass both in excitation and emission modes, the scanning speed was set at 300 nm/min and the PMT voltage was 450 V. Experiments were conducted similarly in 10% and 25% vol DMSO. UV-visible absorption spectra were acquired with a DR6000 UV-Vis Spectrophotometer (Hach).

Dynamic Light Scattering. DLS measurements were performed on a Zetasizer Nano-Zs (Nanoseries) from Malvern instruments at room temperature. Solutions in water (doubly distilled deionized water) with required concentrations were prepared and filtered through a 0.45 μm Teflon membrane and the first 2.5 mL of solutions were discarded to avoid possible contamination from the filters. The polystyrene latex model (RI: 1.590 and absorption: 0.01) was chosen (the one giving the most reproducible results within a large series of replicates) measuring at 173° (backscatter (NIBS default)) with an automatic adjustment of experiment duration. The results were analyzed using the Zetasizer software (v 6.01) from Malvern Instruments. The results shown are the most representative over a series of at least 8 measurements which are each the average of at least 13 runs of ≥ 10s. The cumulant analysis was considered when possible together with the distribution analyses.

Scanning Electron Microscopy for LFD-01. Low and high-resolution micrographs of samples on vitreous carbon were acquired with a scanning electron microscope (SEM) JEOL JSM-6320F at 15kV. Concentrations are given in the paper and in the present document where the images appear. Ultrasound was produced at a frequency of 40 kHz, and a power comprised between 0.25 and 1 W/cm^2.

Transmission Electron Microscopy for LFD-01. The samples were deposited on carbon-coated copper grids and were characterized with a transmission electron microscope (TEM) JEOL JEM 2011. Concentrations are given in the paper and in the present document where the images appear. Ultrasound was produced at a frequency of 40 kHz, and a power comprised between 0.25 and 1 W/cm^2.

Scanning Electron Microscopy (PhePhe dipeptide). 1.93 mL of a solution of LFD-**01** (0.105 mM, final concentration 0.1 mM) was added to a glass vial containing 2.5 mg of PhePhe (final concentration 4 mM) followed by the addition of 70 μL of water to complete the volume to 2 mL. After ultrasound for 15 seconds (ultrasound cleaner bath Bandelin Sonorex, frequency 35 kHz, and power 215/860 W), the precipitate and the solution were deposited using a Pasteur pipette on a double-sided adhesive carbon tape before drying at room temperature for 20 minutes and gold staining prior to images acquisition. SEM images (PhePhe) were acquired using a FEI XL30 ESEM microscope (formerly Philips) in high vacuum mode (SE detector) by secondary electrons and using an acceleration voltage of 20 kV.

Environmental-SEM. For a final volume of 400 μL, 385.6 μL of water and 14.4 μL of NaOH (1M, 36 mM final concentration) were added to 0.8 mg of Fmoc-Leu-Leu (final concentration, 4 mM) before vortexing for 30 seconds. This was repeated adjusting the weighted mass of Fmoc-Leu-Leu to 2.3 mg for the 12 mM concentration. For the 36 mM sample, a final volume of 200 μL was considered. 192.8 μL of water and 7.2 μL of NaOH (1M, 36 mM final concentration) were added to 3.4 mg of Fmoc-Leu-Leu before vortexing for 30 seconds. An aging time comprised between 2 and 5 hours was considered for all images. The samples were deposited on a double-sided adhesive carbon tape before introduction in the vacuum chamber. ESEM images (Fmoc-Leu-Leu) were acquired with a FEI XL30 ESEM microscope (formerly Philips) in environmental mode (Low vacuum, GSE detector) at a temperature of 8°C (Peltier cooled stage) starting with 100% humidity under 8.3 torr and ending at 2.2 torr and 20.5% humidity and using an acceleration voltage of 20 kV.

Confocal fluorescence microscopy. Fmoc-Leu-Leu samples (4, 12 and 36 mM) were prepared exactly as for the Environmental-SEM experiments (see above) except that the water added was replaced by a solution of LFD-**01** at 0.105 mM concentration (prepared using ultrasound for 2 minutes: ultrasound cleaner bath Bandelin Sonorex, frequency 35 kHz, and power 215/860 W) so that the final concentration is 0.1 mM after dilution. The sample prepared using PhePhe was identical to the one prepared for SEM (see above). The samples were deposited on glass microscope slides and imaged directly at room temperature. Confocal microscopy images were acquired using a Zeiss LSM 710 microscope (Axis Observer, inverted objective) with a Plan-Apochromat 100×/1.40 Oil DIC M27, a pinhole comprised between 46.33 and 301.93 μm with λ_{exc} = 458 or 488 nm and λ_{em} = 519 or 527 nm. Alginate solutions, without and with Ca^{2+} ions were prepared as described in the UV and fluorescence section (see above). Confocal images were very similar when comparing samples prepared either by (i) injecting the alginate/LFP-**01** solutions directly inside 5% wgt Ca^{2+} solutions (UV and fluorescence section) and (ii) depositing the Ca^{2+} solution on the top of the alginate/LFP-**01** solution for slow Ca^{2+} diffusion (the alginate/LFP-**01** solution is very viscous).

DFT calculations. Molecular electrostatic potential surface was calculated on solvent-accessible surface[6] with a standard probe sphere radius of 1.2 Å. Atomic charges were calculated at B3LYP/6-31G(d) level of theory with the CPCM water model[7] according to the CHelpG scheme.[8] DFT calculations were performed with the Gaussian09 Rev.D01 package.[9] All the structures were fully optimized at the B3LYP/6-31G(d) level of theory using a water continuum model (CPCM) and frequency checked for true minimas. BSSE corrections were applied using the counterpoise method, without solvent, for calculation of the energy corresponding to the lowest energy found after minimization. For more details see the end of this document.

Synthesis of (*E*)-1-methyl-4-(2-(9-octyl-9*H*-carbazol-3-yl)vinyl)pyridin-1-ium iodide (LFD-01). LFD-**01** was prepared in a two-step synthesis (see Supplementary Fig. 1), consisting first in alkylating picoline with methyl iodide followed in second step in the Knoevenagel condensation of the picolinium salt with 9-octyl-9*H*-carbazole-3-carbaldehyde. The dye was obtained in 92% yield for the two steps and the sole condensation product detected by NMR was the *E*-isomer, in agreement with what was previously reported in the literature.[10,11,12]

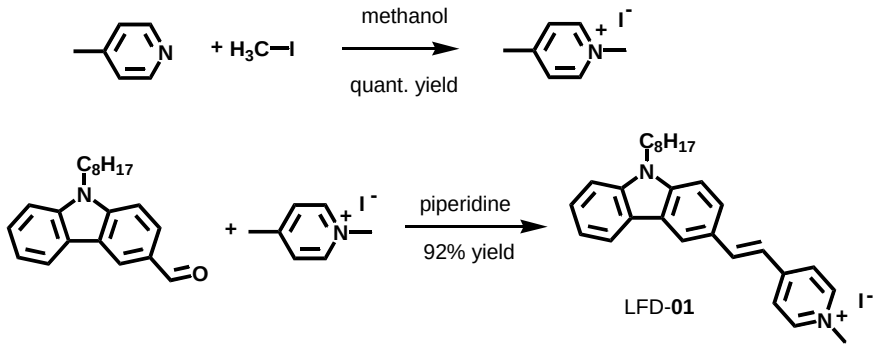

Figure S1. Synthetic route for LFD-**01**.

Methyl iodide (0.85 g, 0.36 mL, 6 mmol) was slowly added to 4-picoline (0.56 g, 0.58 mL, 6 mmol). A white precipitate formed immediately and the stirring was maintained for 15 min. Methanol (6 mL) was then added, followed by 9-octyl-9*H*-carbazole-3-carbaldehyde (1.84 g, 6 mmol) and piperidine (0.6 mL). The reaction mixture was refluxed for 24 h. The solvent was removed under reduced pressure. Addition of methanol precipitated a light yellow solid. The solid was filtered off and washed with ether until no color was visible in the filtrate. It was used without any further purification (2.89 g, 92% yield). ^{1}H NMR (400 MHz, DMSO-d_6, ppm): 0.81 (t, 3H, J = 6.4 Hz), 1.18-1.26 (m, 10H), 1.76-1.78 (m, 2H), 4.24 (s, 3H), 4.43 (t, 2H, J = 6.2 Hz), 7.28 (t, 1H, J = 7.3 Hz), 7.51-7.56 (m, 2H), 7.65 (d, 1H, J = 8.1 Hz), 7.72 (d, 1H, J = 8.1 Hz), 7.89 (d, 1H, J = 8.2 Hz), 8.18-8.24 (m, 4H), 8.59 (s, 1H), 8.81 (d, 2H, J = 5.9 Hz); ^{13}C NMR (100 MHz, DMSO-d_6, ppm): 13.9, 22.0, 26.4, 28.47, 28.54, 28.65, 31.1, 42.4, 46.6, 109.9, 110.0, 119.6, 119.9, 120.4, 121.1, 122.0, 122.6, 122.7, 126.1, 126.2, 126.5, 140.6, 141.4, 142.3, 144.7, 153.1; HRMS (ESI MS) m/z: theor: 397.2638 found: 397.2635 ([M]$^+$ detected). Elemental analysis for LFD-**01**+0.3 H_2O. Calc. (Found): C 63.47 (63.45), H 6.39 (6.31), N 5.29 (5.34).

Synthesis of (*E*)-1-methyl-4-(2-(9-methyl-9*H*-carbazol-3-yl)vinyl)pyridin-1-ium iodide (LFD-02).

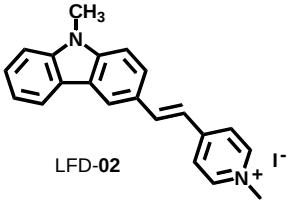

Figure S2. Molecular structure of LFD-**02**.

Iodomethane (0.85 g, 0.37 mL, 6 mmol) was slowly added to 4-picoline (0.558 g, 6 mmol). A white precipitate formed immediately and the stirring was maintained for 15 min. 6 mL of methanol were then added, followed by 9-methyl-9*H*-carbazole-3-carbaldehyde (1.25 g, 6 mmol) and piperidine (0.6 mL). The reaction mixture was refluxed for 24 h. The solvent was removed under reduced pressure. Dissolution in acetonitrile followed by precipitation in diethyl ether precipitated a yellow solid that was filtered off, washed several times with

ether and dried under vacuum (2.10 g, 82% yield). ^{1}H NMR (DMSO-d_6): 3.93 (s, 3H), 4.24 (s, 3H), 7.30 (t, 1H, J = 7.4 Hz), 7.50-7.56 (m, 2H), 7.65 (d, 1H, J = 8.2 Hz), 7.72 (d, 1H, J = 8.6 Hz), 7.91 (dd, 1H, J = 1.1 Hz, J = 8.6 Hz), 8.17-8.23 (m, 4H), 8.59 (s, 1H), 8.80 (d, 2H, J = 6.6 Hz). ^{13}C NMR (DMSO-d_6): 29.2, 46.6, 109.7, 109.9, 119.7, 119.9, 120.3, 121.0, 121.9, 122.5, 122.7, 126.1, 126.2, 126.4, 141.2, 141.9, 142.3, 144.7, 153.0. ESI(+)-MS m/z : 299.2 (1 peak). HRMS (ESI MS) m/z theor: 299.1543 found: 299.1539 ([M]$^{+}$ detected). Elemental analysis for LFD-**02**+0.3 H_2O. Calc. (Found): C 58.43 (58.46), H 4.58 (4.37), N 6.49 (6.44).

Supplementary Discussion

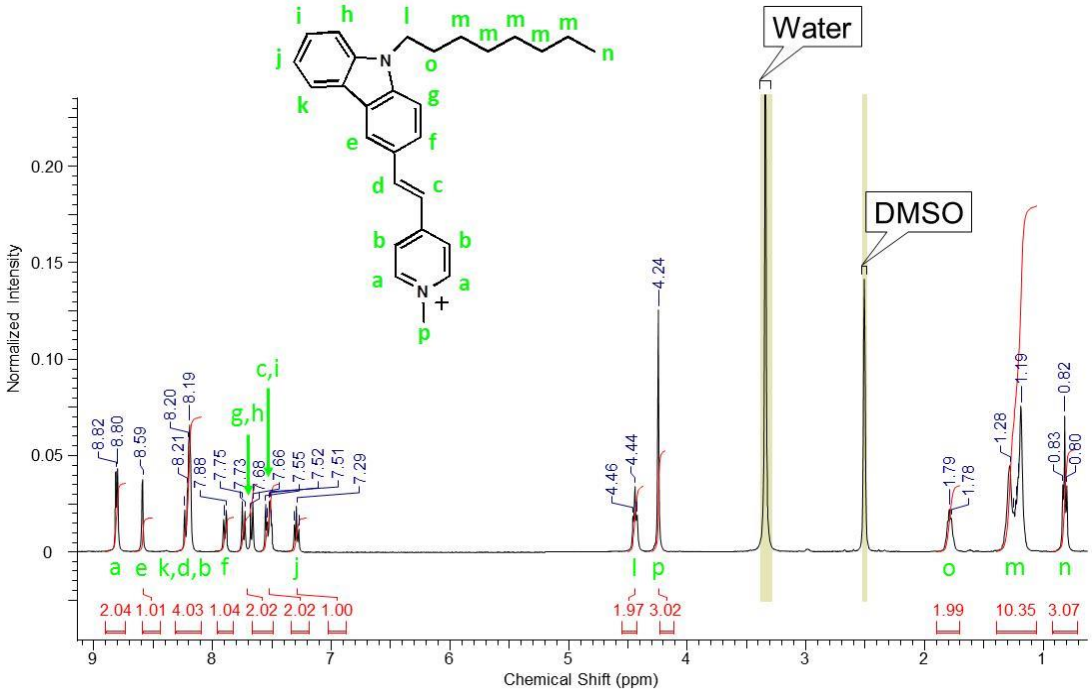

Figure S3. ^{1}H NMR spectrum of compound LFD-**01** in DMSO-d_6.

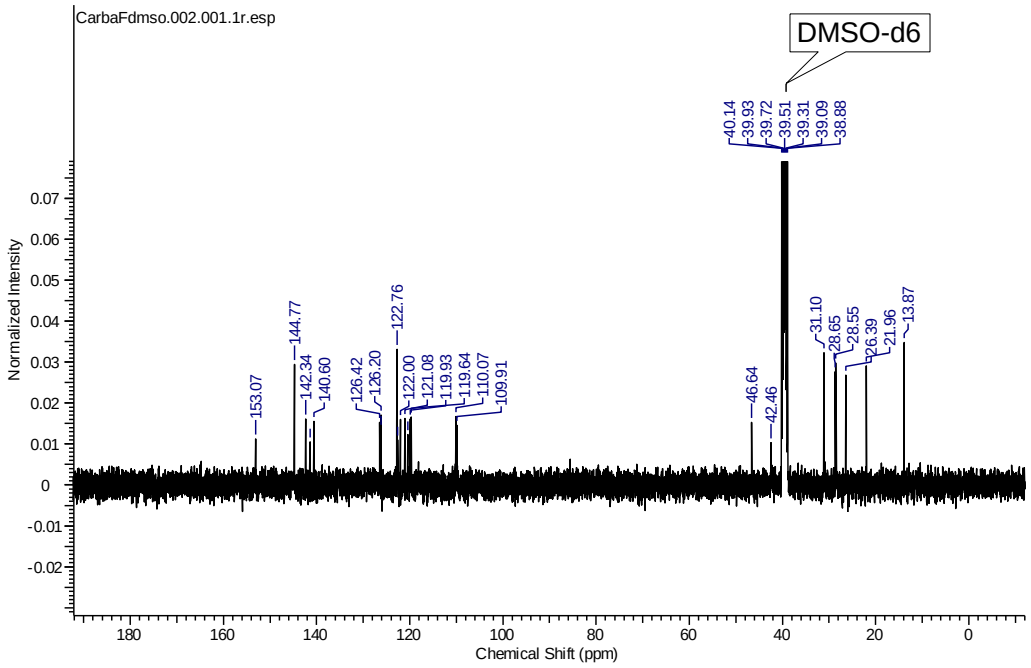

Figure S4. ^{13}C NMR spectrum of LFD-**01** in DMSO-d_6.

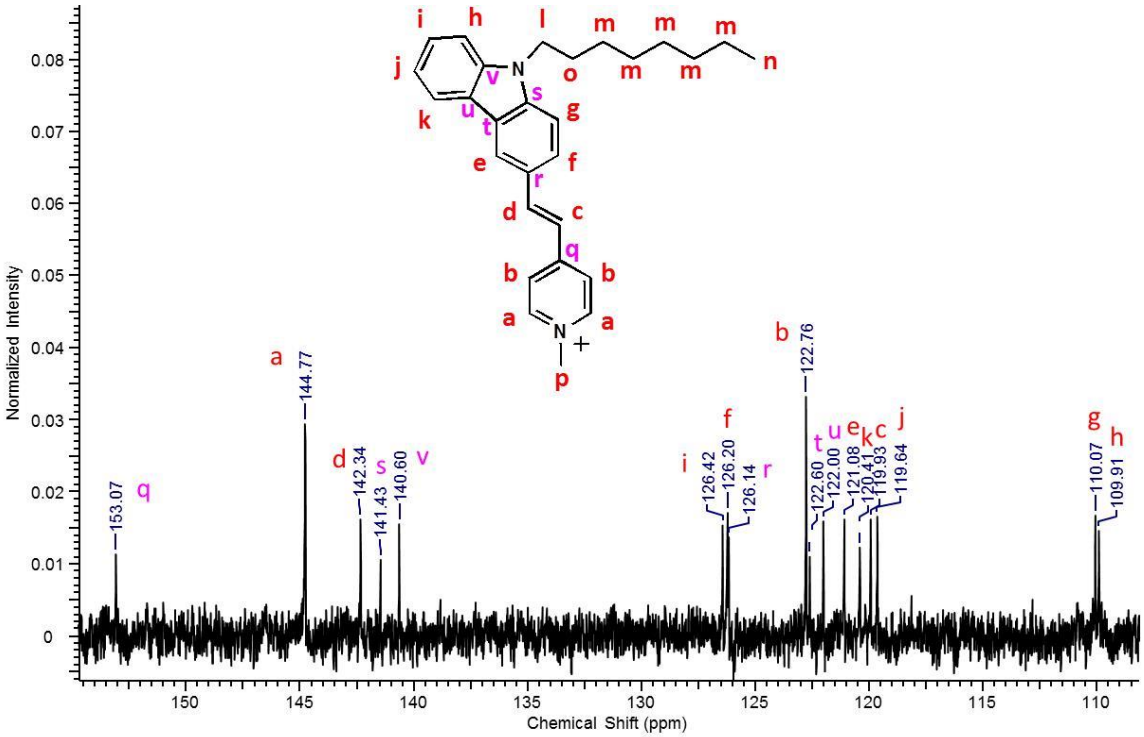

Figure S5. Excerpt of the ^{13}C NMR spectrum of LFD-**01** in DMSO-d_6.

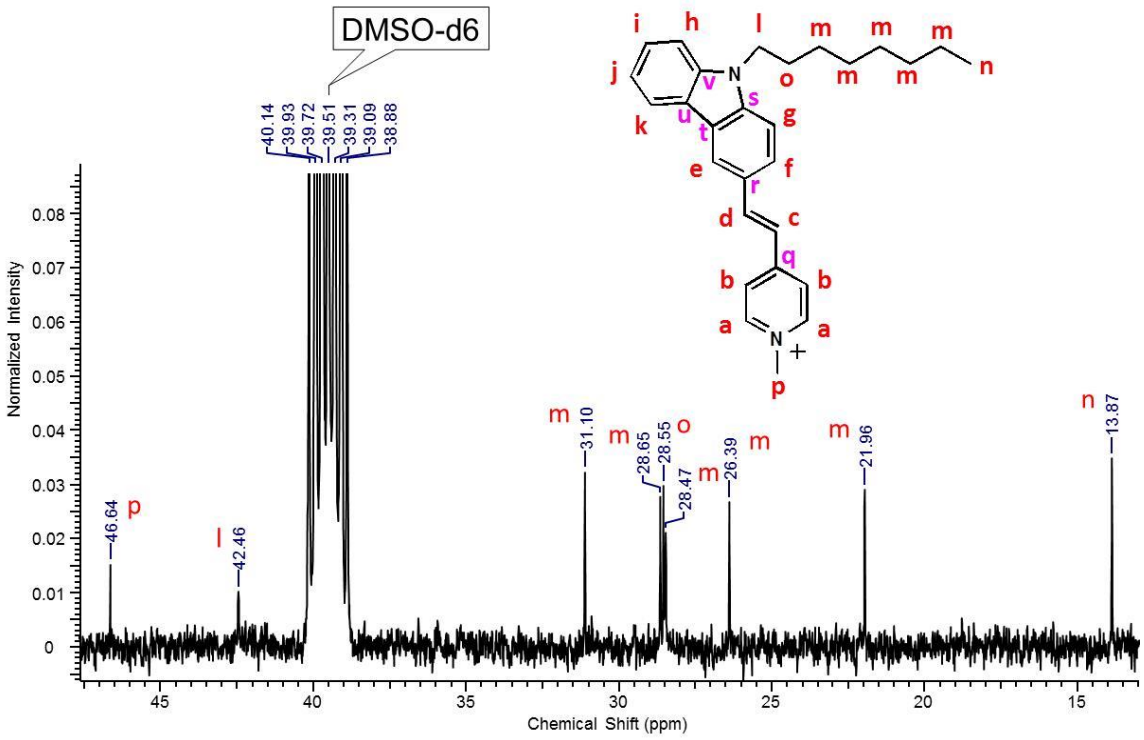

Figure S6. Excerpt of the ^{13}C NMR spectrum of LFD-**01** in DMSO-d_6.

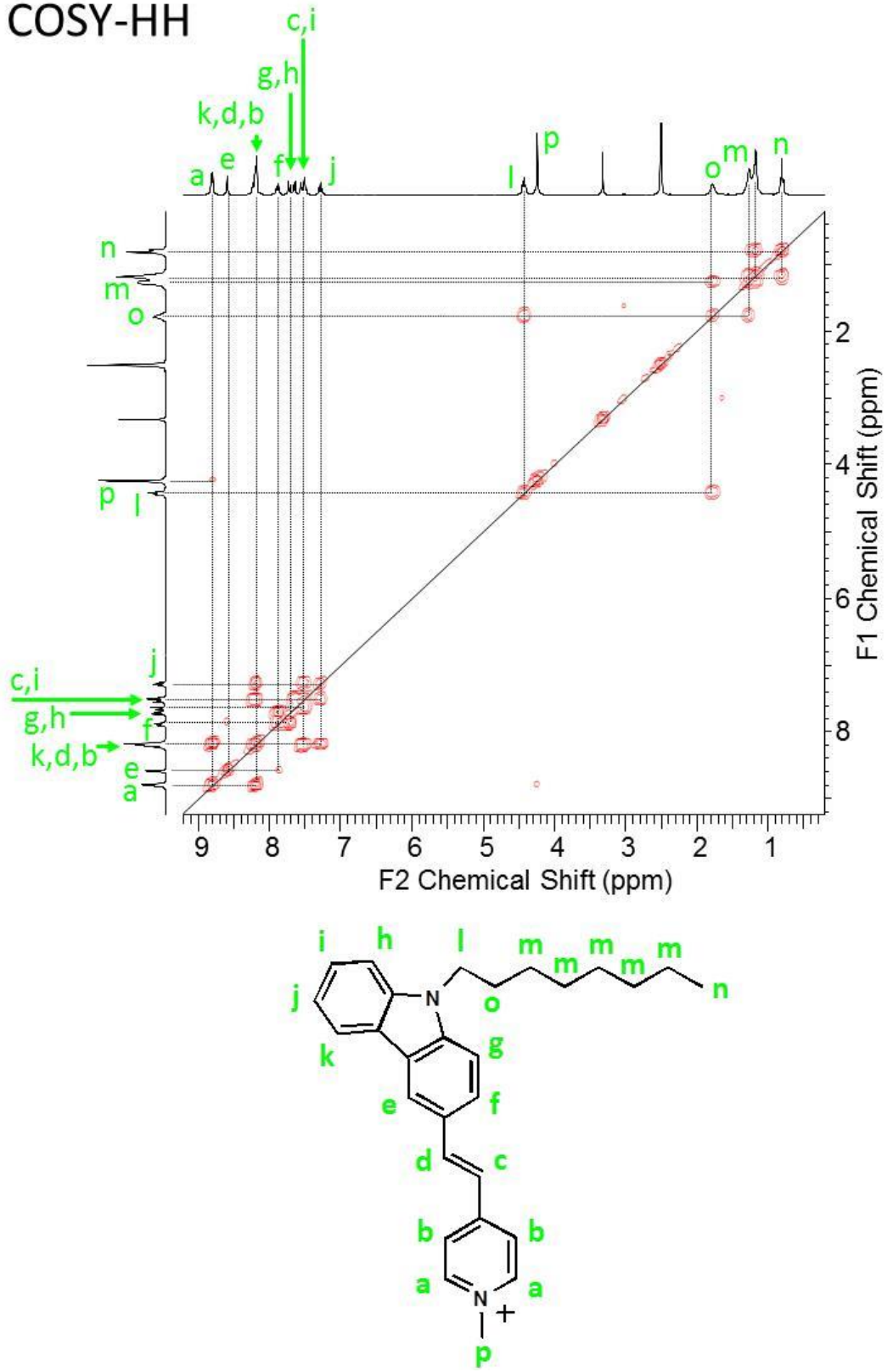

Figure S7. COSY H-H NMR spectrum of LFD-**01** in DMSO-d_6.

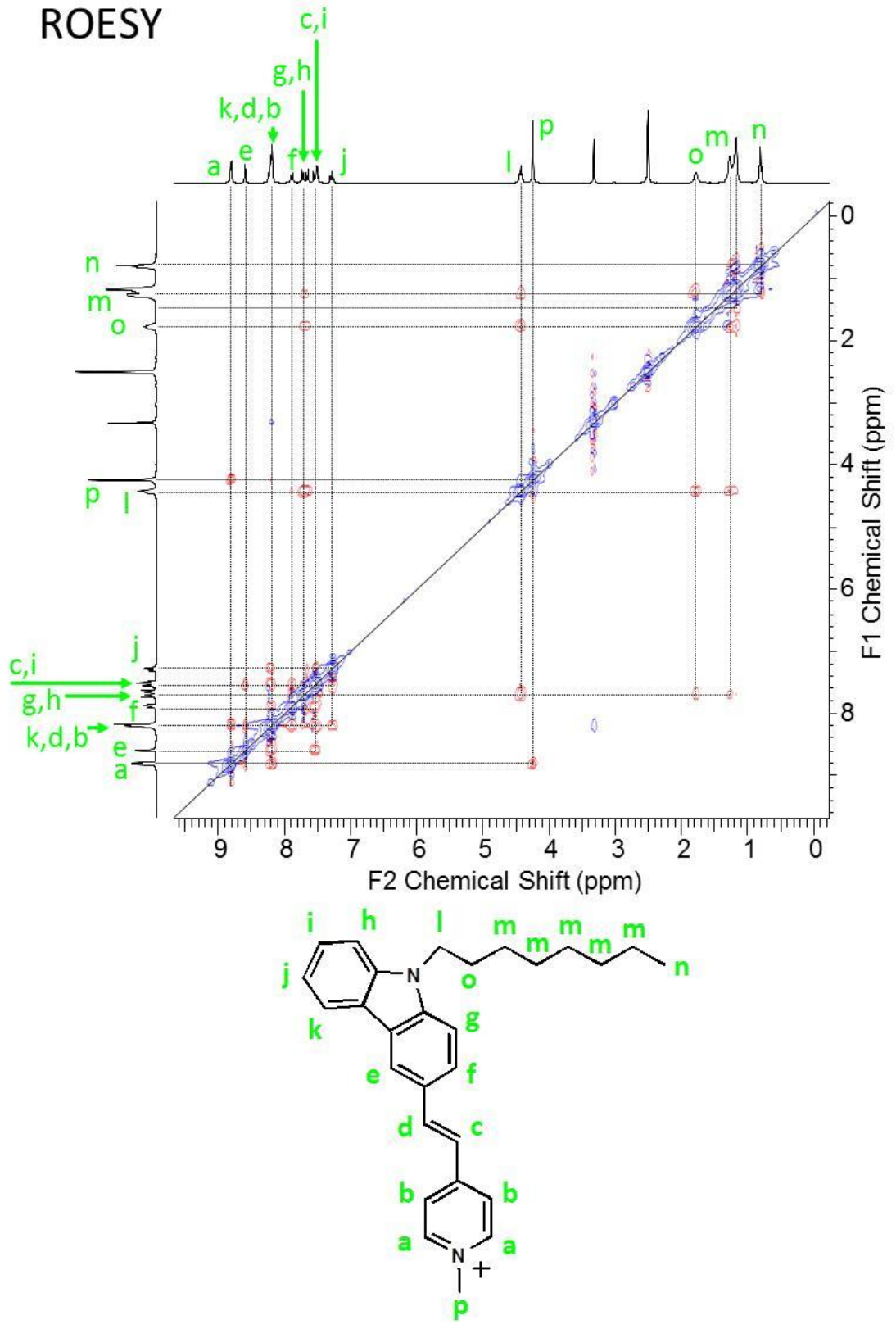

Figure S8. 2D-ROESY NMR spectrum of LFD-**01** in DMSO-d_6.

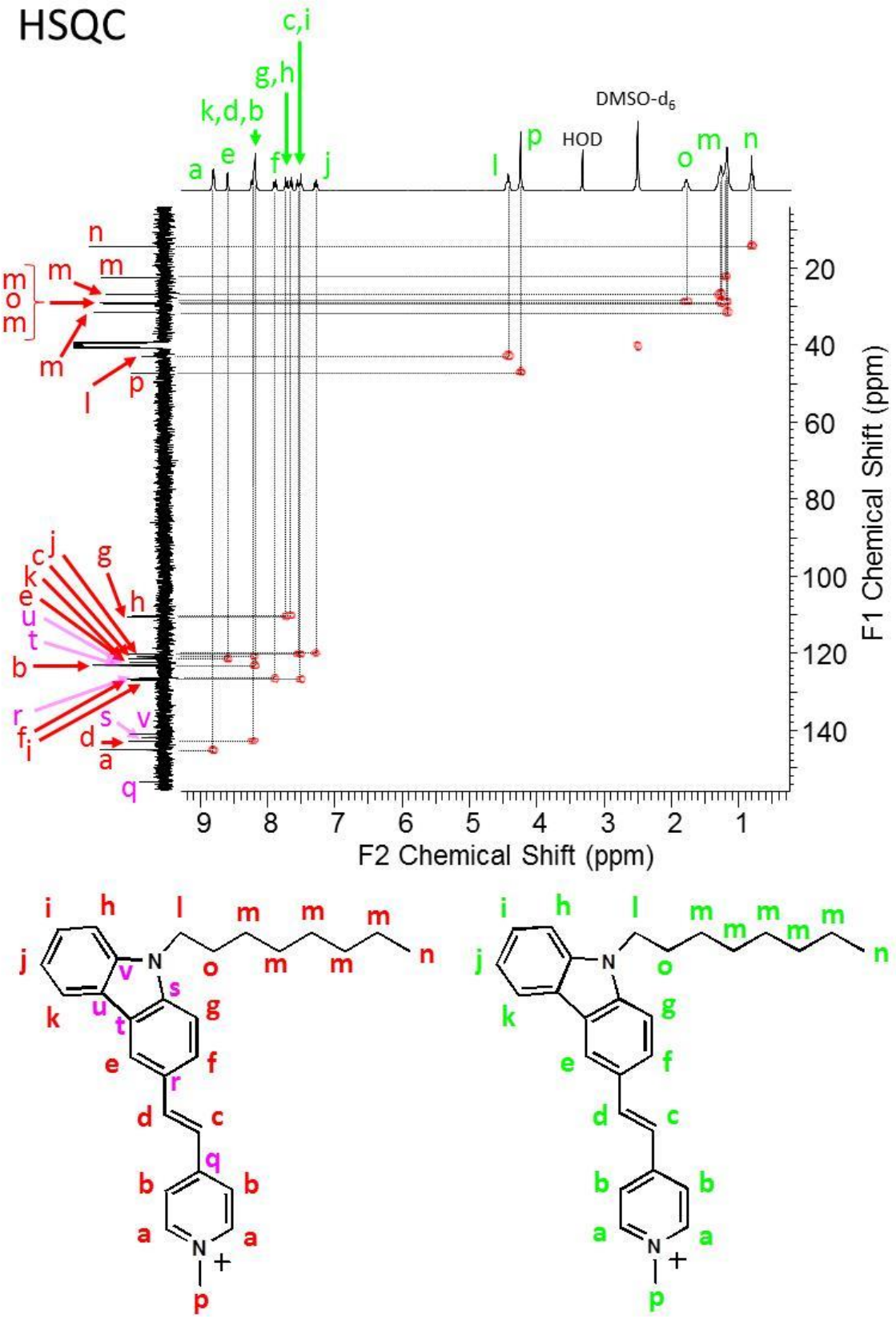

Figure S9. HSQC NMR spectrum of LFD-**01** in DMSO-d_6.

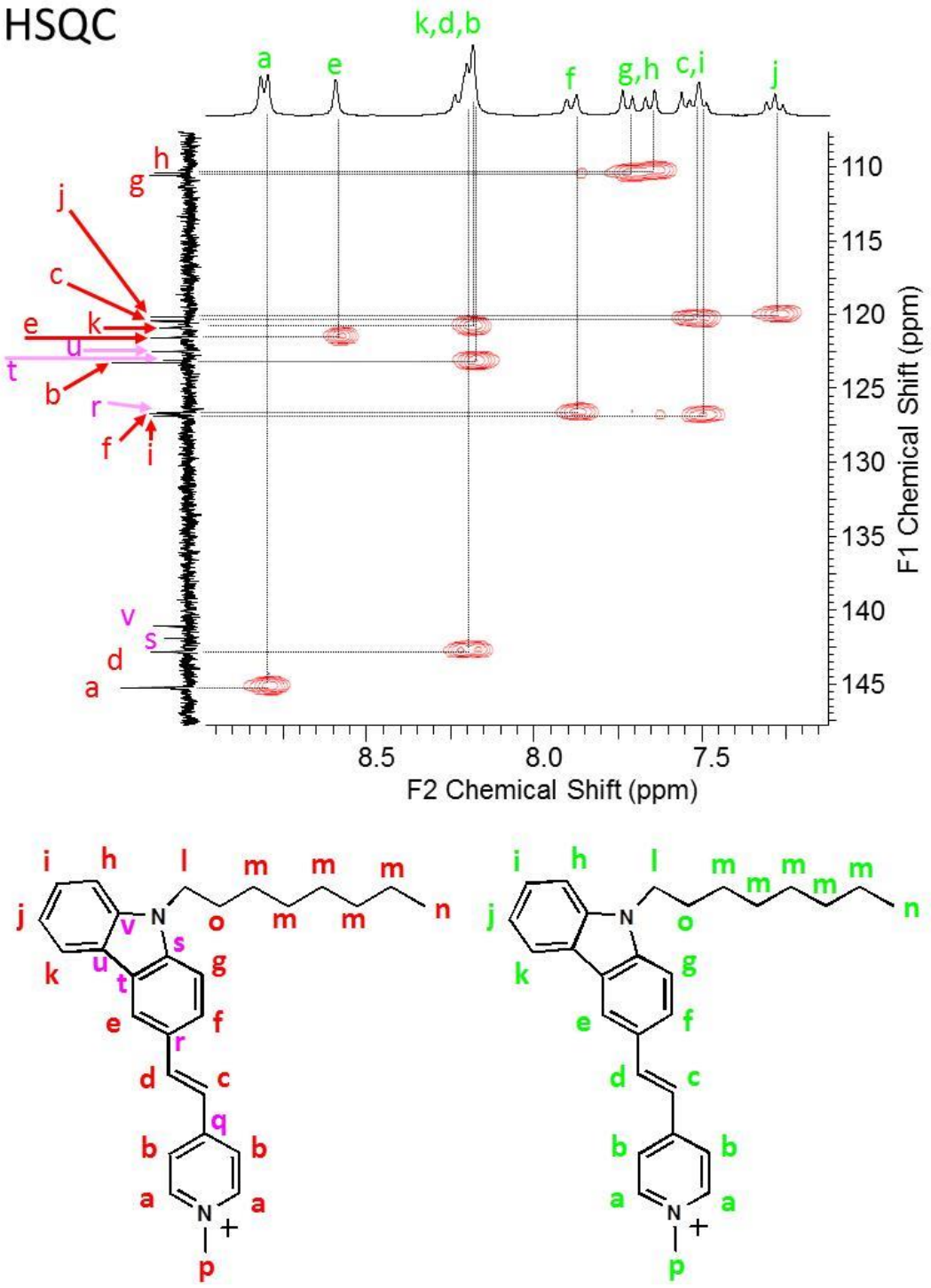

Figure S10. Excerpt of the HSQC NMR spectrum of LFD-**01** in DMSO-d_6.

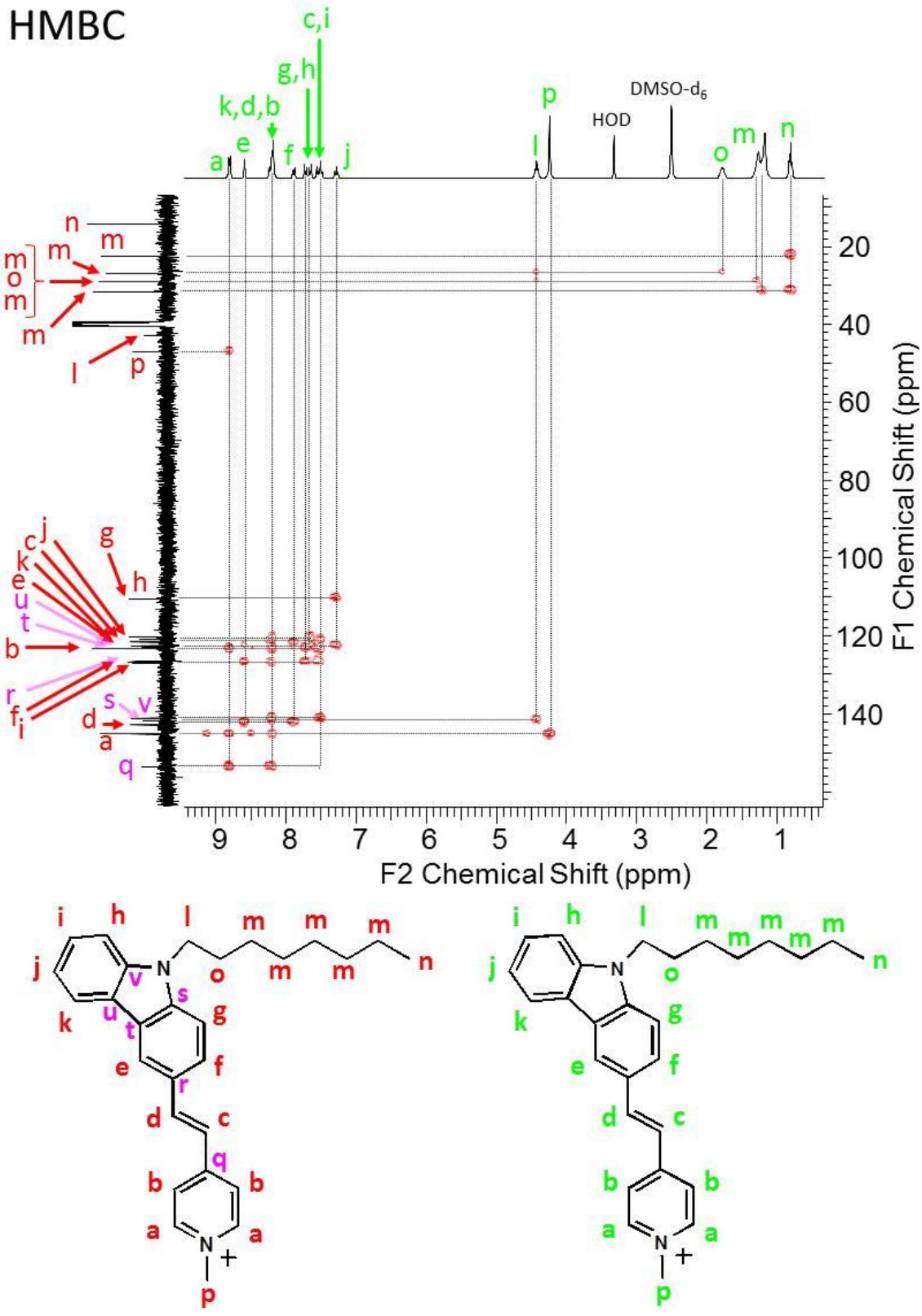

Figure S11. HMBC NMR spectrum of LFD-**01** in DMSO-d_6.

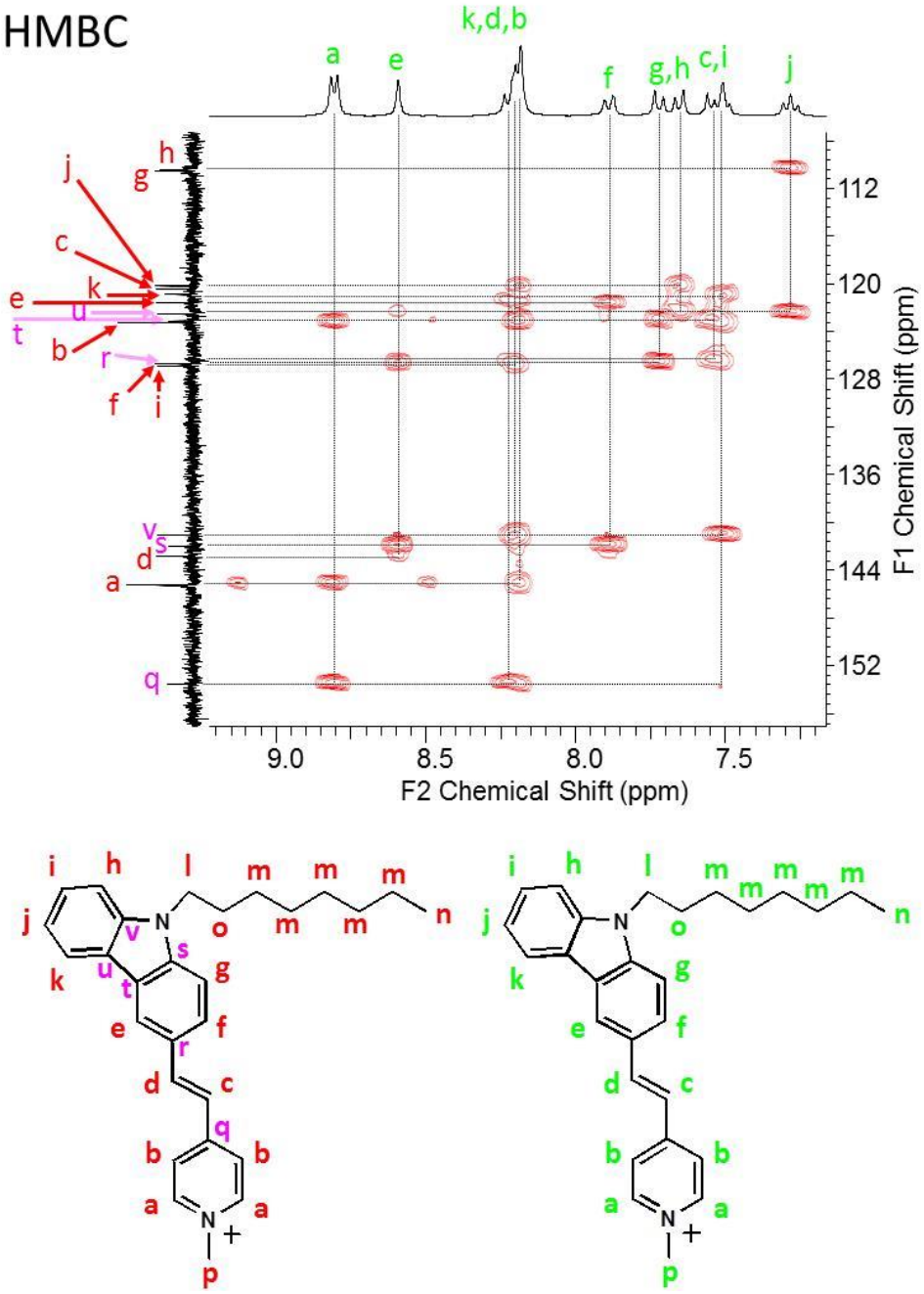

Figure S12. Excerpt of the HMBC NMR spectrum of LFD-**01** in DMSO-d_6.

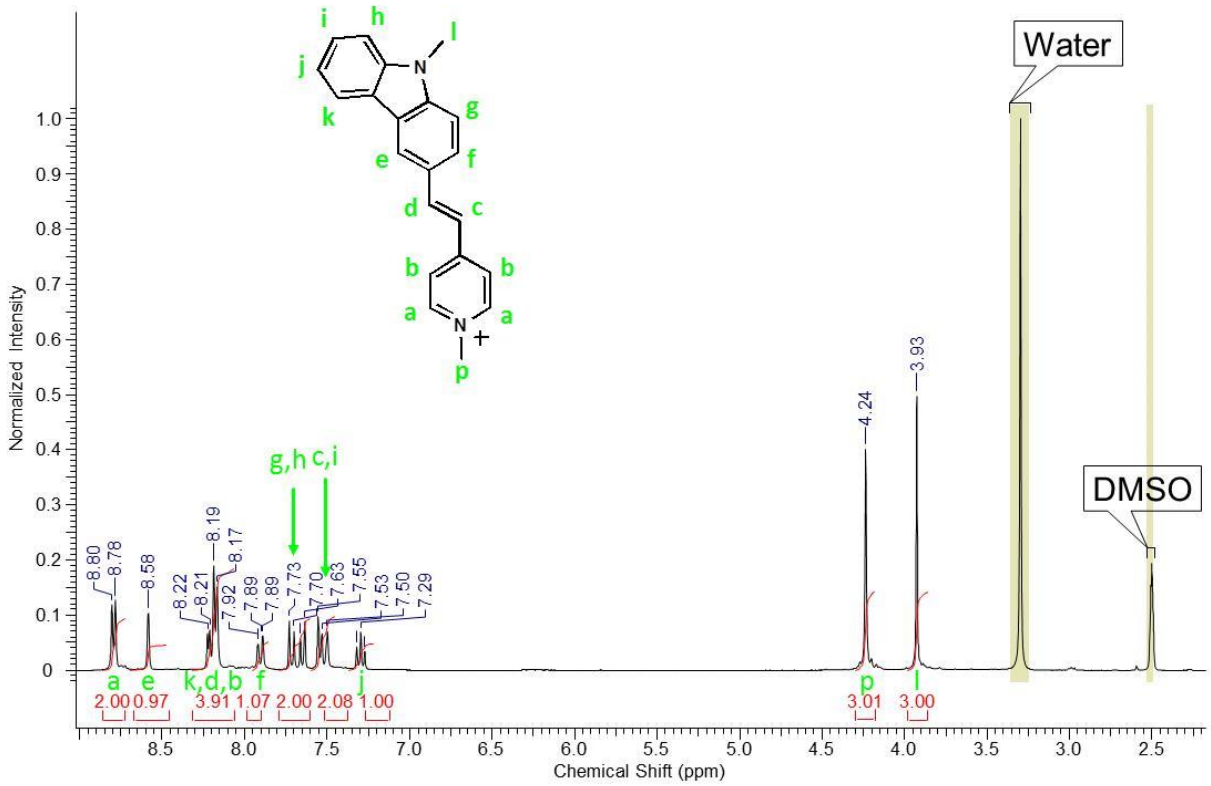

Figure S13. ^{1}H NMR spectrum of compound LFD-**02** in DMSO-d_6.

The asignment of the ^{1}H-NMR spectrum was based on the one done for LFD-**01** as the chemical shifts are almost identical to those of LFD-**01**. The ^{13}C-NMR (see Supplementary Fig. 14), DEPT-135 and COSY-HH spectra are also in agreement with the proposed structure for LFD-**02** and also in agreement with the corresponding experiments for LFD-**01**.

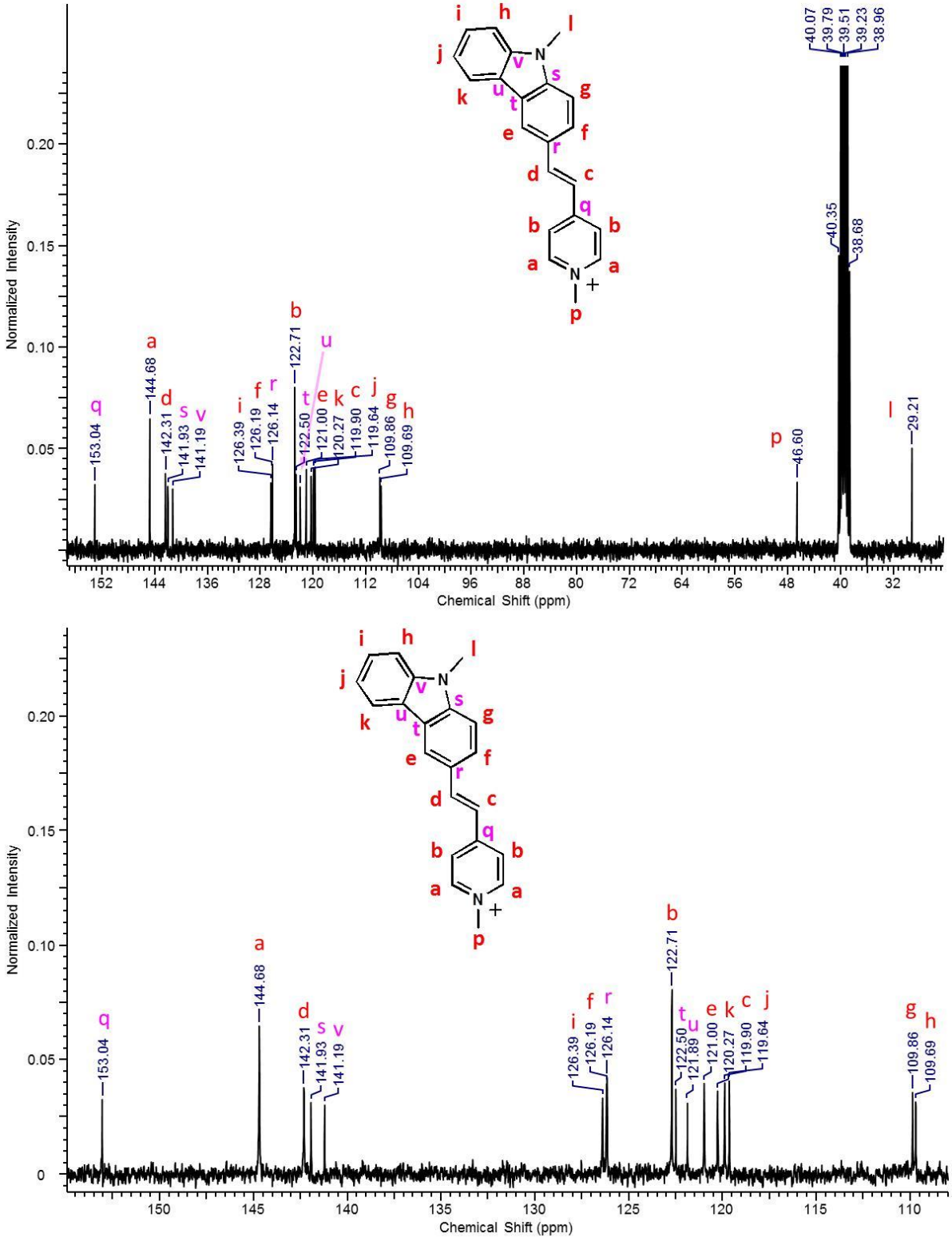

Figure S14. ^{13}C NMR spectrum (and excerpt, bottom) of LFD-**02** in DMSO-d_6.

Table S1. λ_{max} for the absorption and the emission of LFD-**01** and corresponding absolute quantum yield in various solvents and at several excitation wavelengths.

Solvent	Φ^a	emission peak (nm)	maximum absorption (nm)	Φ	emission peak (nm)
Acetone	0.317	596	431	0.313 (exc 430)	593
Acetonitrile	0.294	594	431	0.291 (exc 430)	597
Chloroform	0.140	600	462	0.140 (exc 460)	600
Dichloromethane	0.134	592	475	0.155 (exc 470)	593
DMF	0.376	593	430	0.369 (exc 430)	593
DMSO	0.443	593	430	0.440 (exc 430)	595
Ethanol	0.350	588	443	0.347 (exc 440)	590
Methanol	0.273	590	436	0.274 (exc 440)	585
THF	0.138	595	440	0.111 (exc 440)	597

a: excitation: 460 nm.

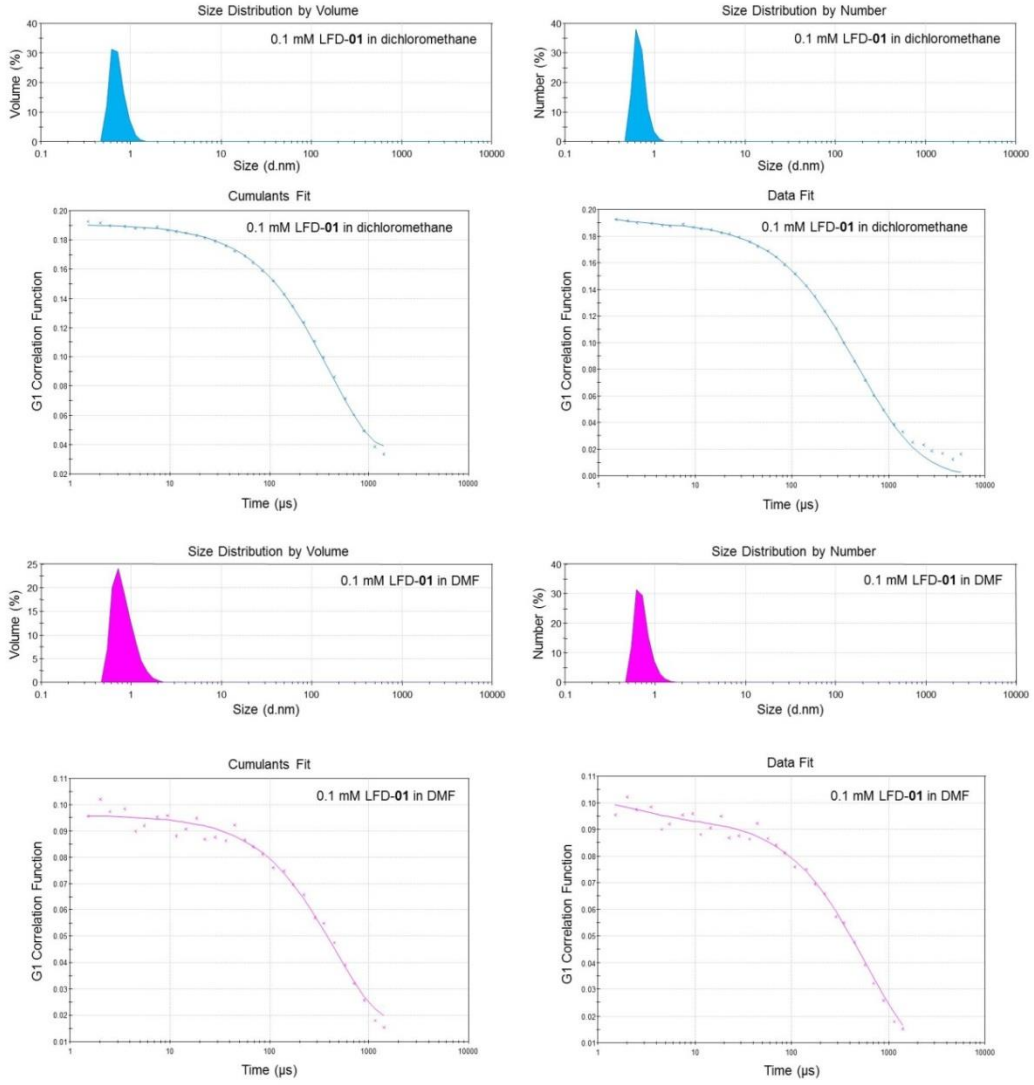

Figure S15. Dynamic Light Scattering (DLS) of LFD-**01** in dichloromethane and in DMF.

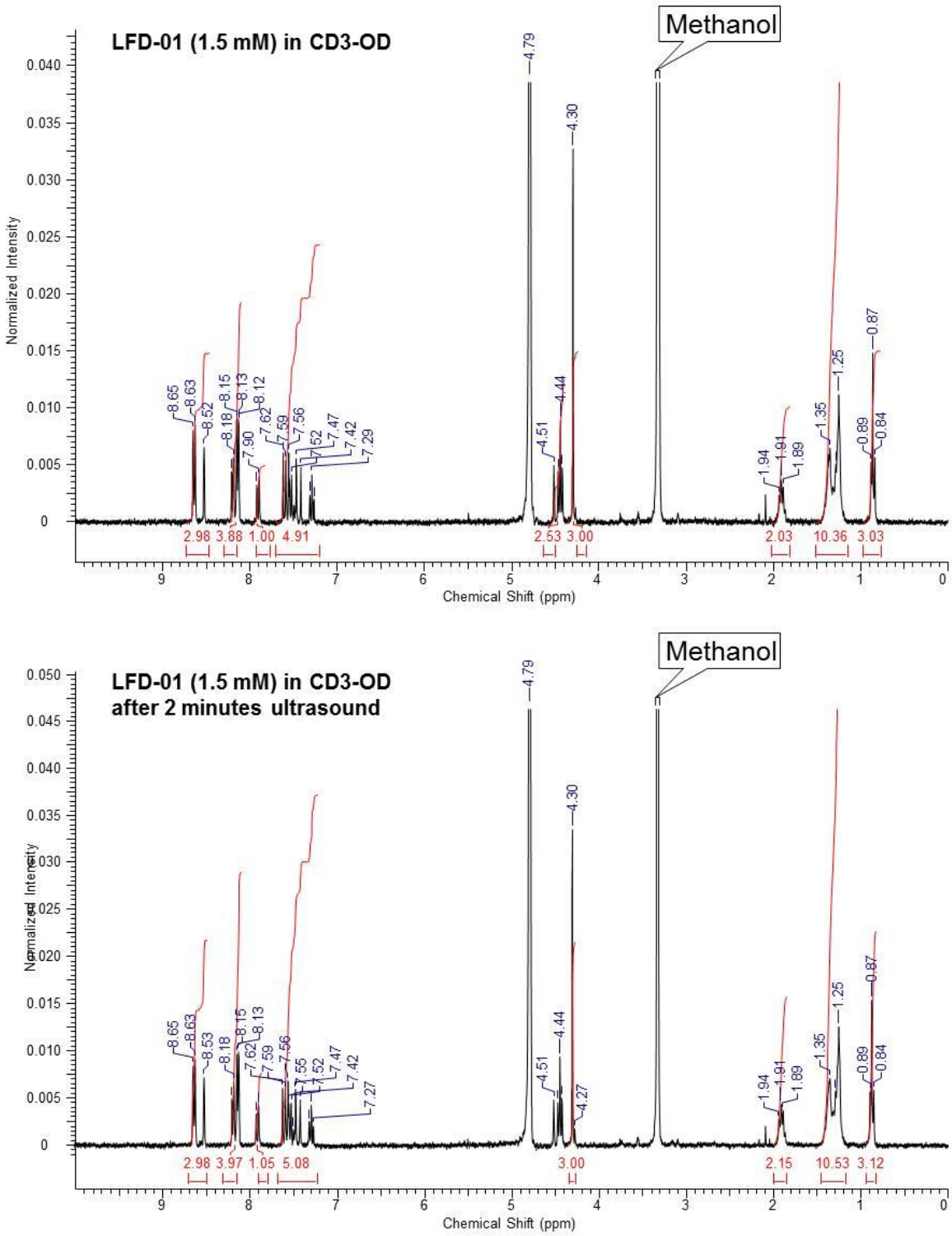

Figure S16. ^{1}H NMR of LFD-**01** in methanol before and after ultrasound for 2 minutes. Results are identical after 10 minutes ultrasound.

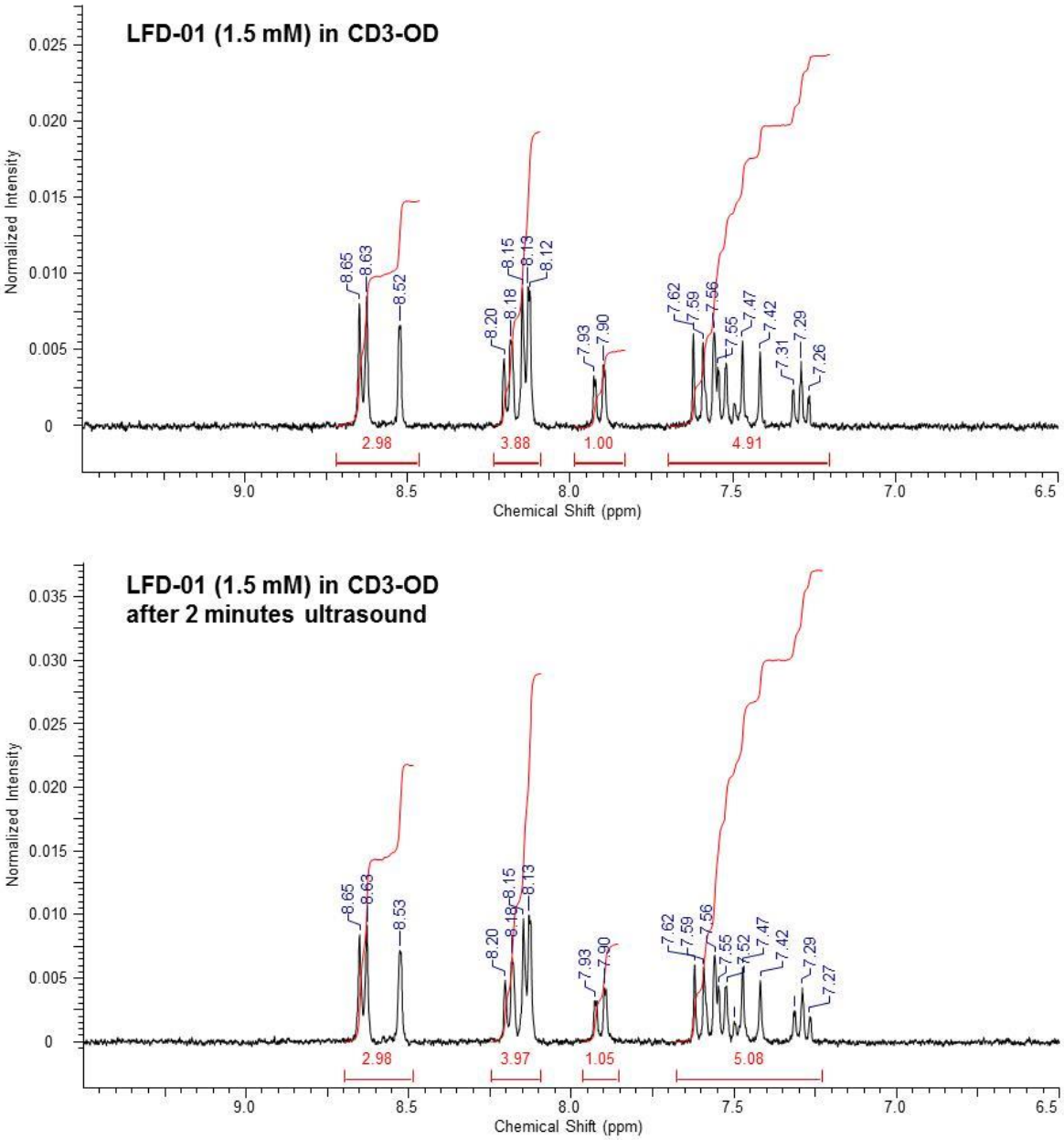

Figure S17. ^{1}H NMR of LFD-**01** in methanol before and after ultrasound for 2 minutes.

Results are identical after 10 minutes ultrasound.

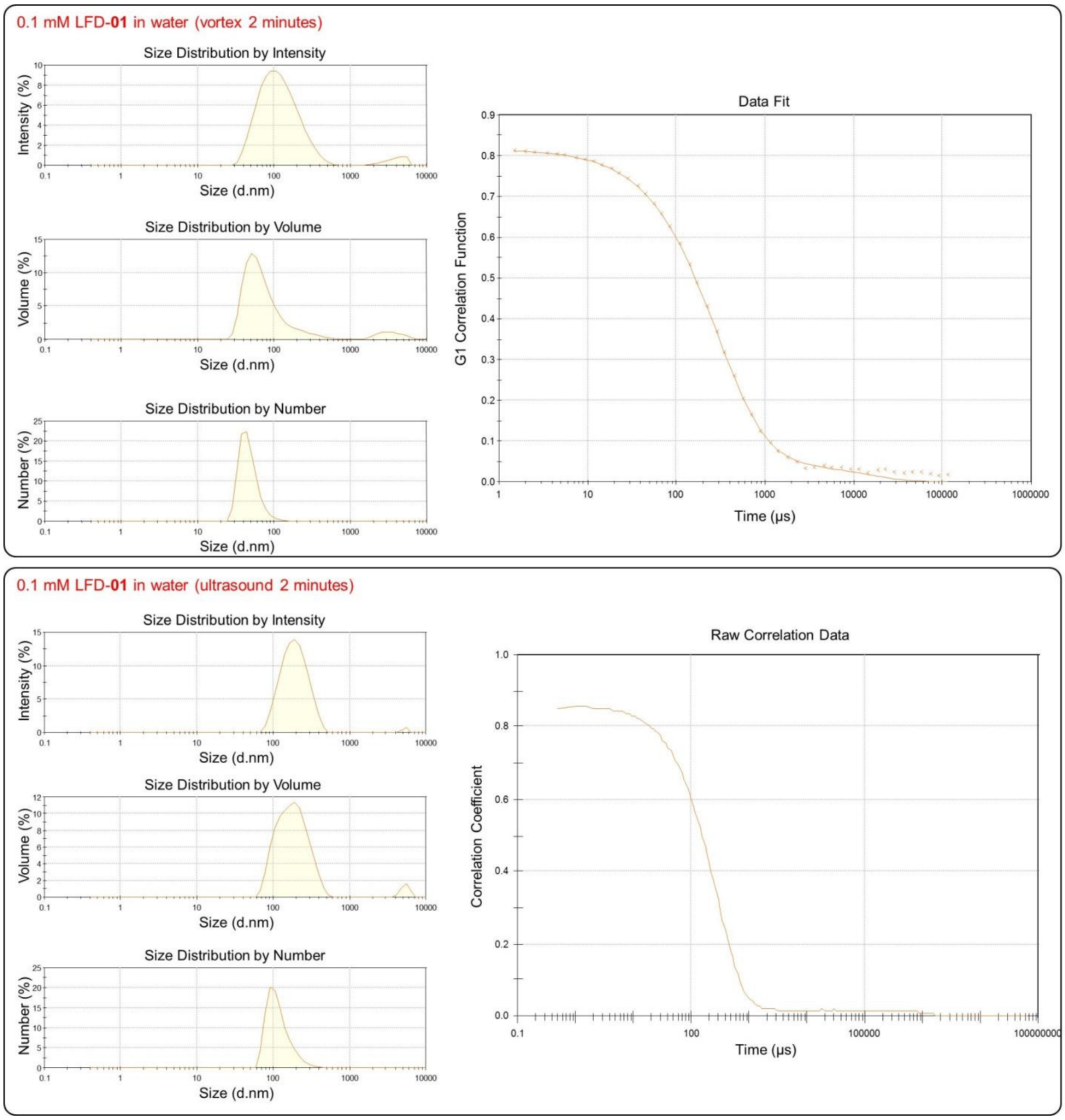

Figure S18. DLS of LFD-**01** in water (0.1 mM) after vortex or ultrasound for 2 minutes.

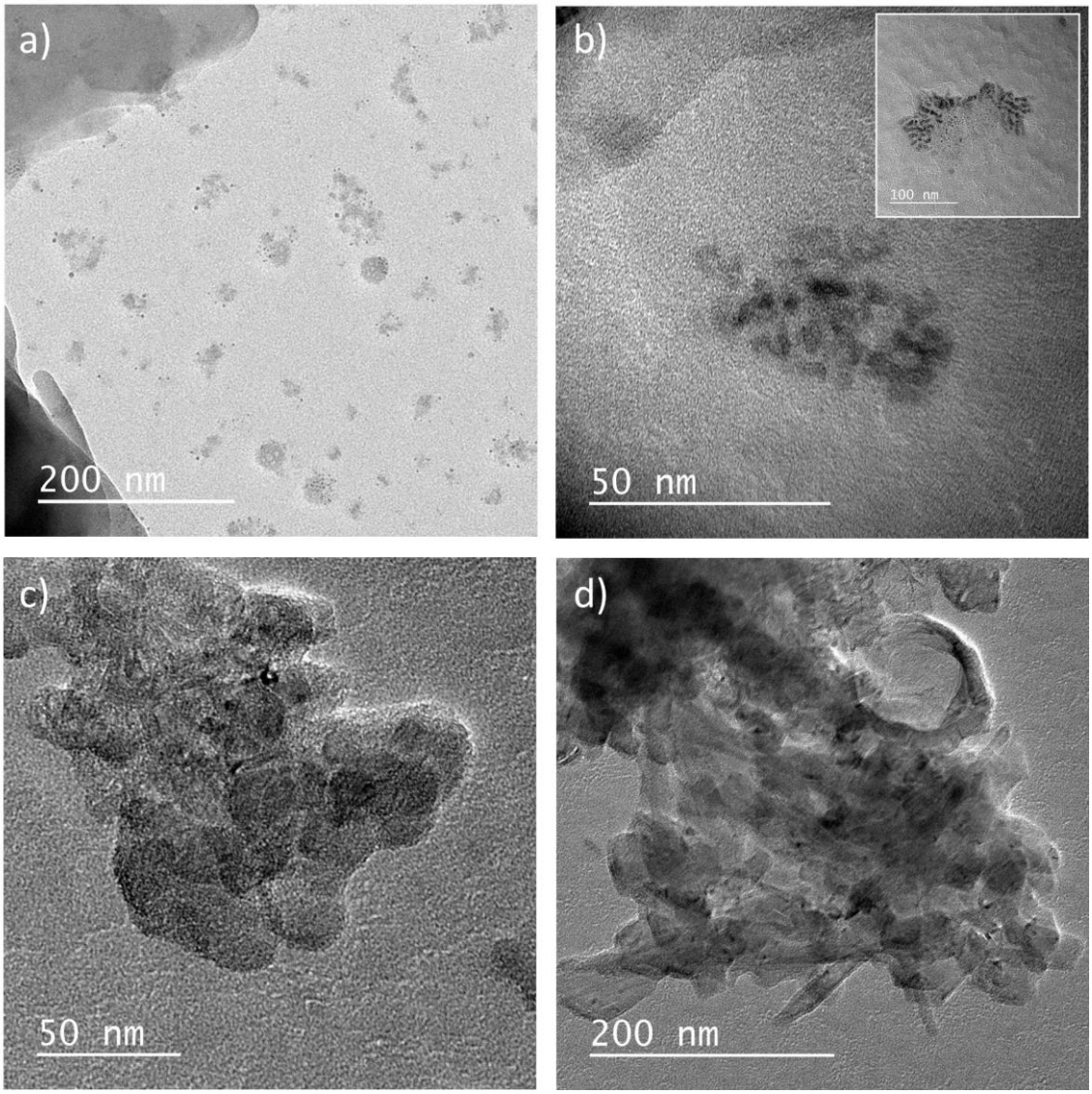

Figure S19. TEM of LFD-**01** in water (0.1 mM) after stirring (vortex, a and b) or ultrasound (c and d) for 2 minutes.

Table S2. Fluorescence quantum yields and emission wavelength for the complexes of LFD-**01** (20 μM fixed concentration) with cucurbiturils.

Compounds	Φ	λ_{exc} (nm)	λ_{em} (nm)	Maximum absorption
LFD-01 (20 μM)	0.021	420	572	415
LFD-01+CB[6] (20 μM)	0.734	450	544	440
LFD-01+CB[7] (800 μM)	0.597	460	580	463
LFD-01+CB[8] (40 μM)	0.338	460	588	481

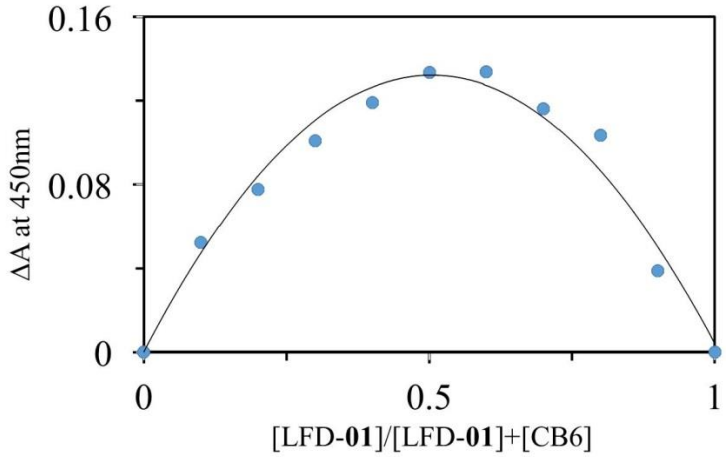

Figure S20. Job Plot for the titration of LFD-**01** with CB[6] in water.

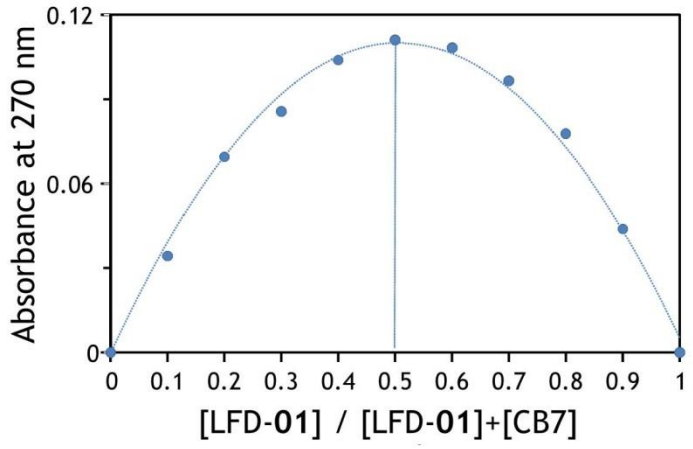

Figure S21. Job Plot for the titration of LFD-**01** with CB[7] in water.

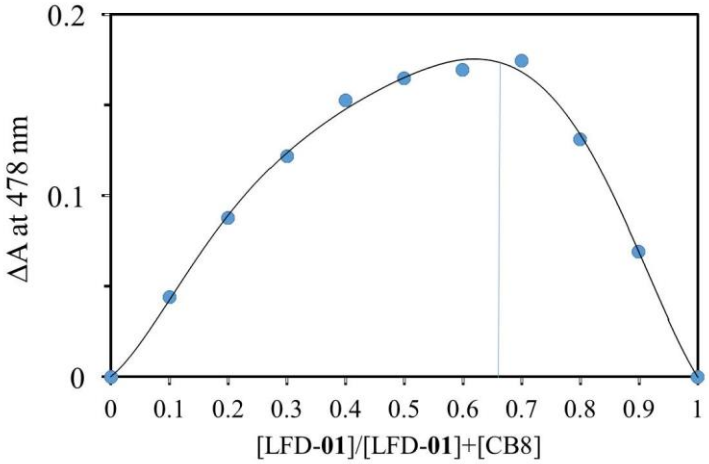

Figure S22. Job Plot for the titration of LFD-**01** with CB[8] in water.

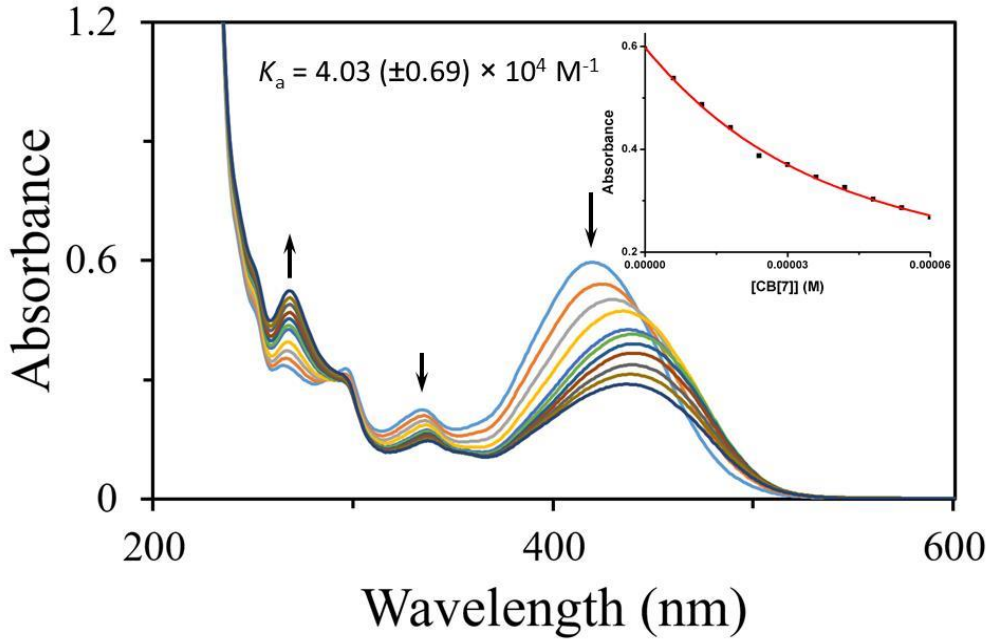

Figure S23. UV-vis titration of LFD-**02** (20 μm) with CB[7] in water.

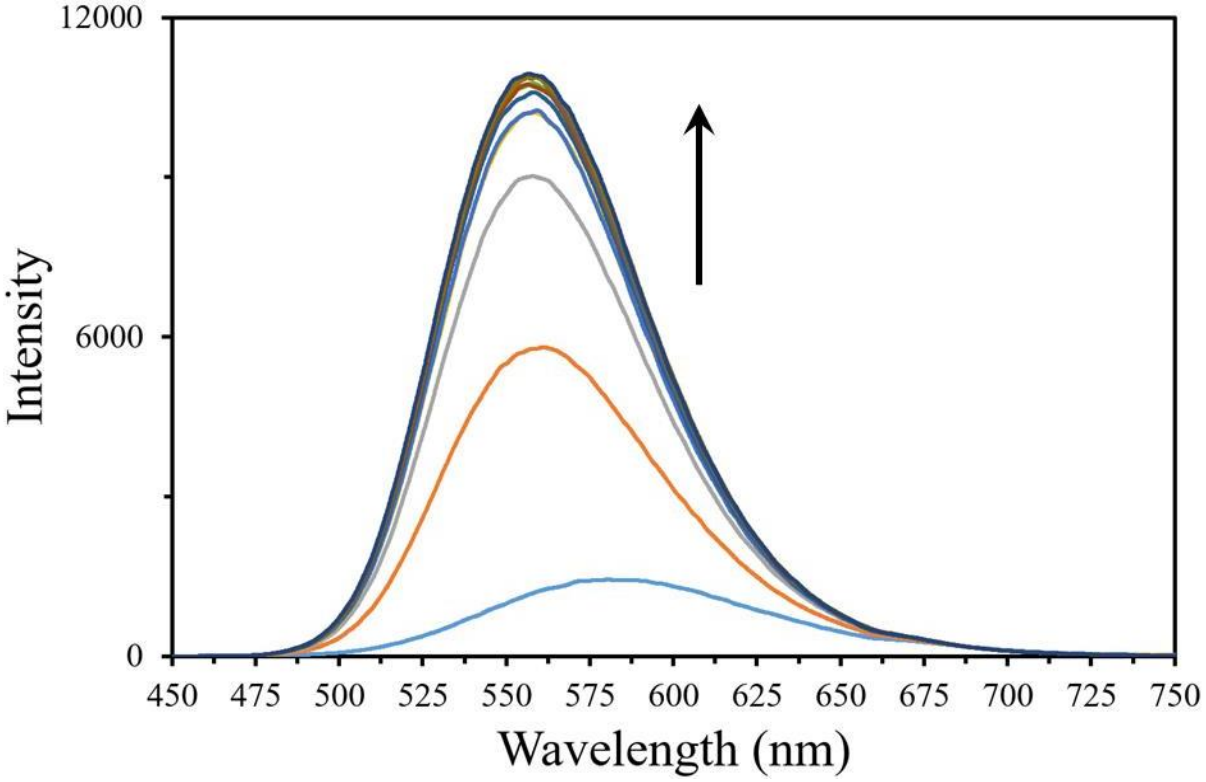

Figure S24. Fluorescence titration of LFD-**02** (20 μm) with CB[7] in water.

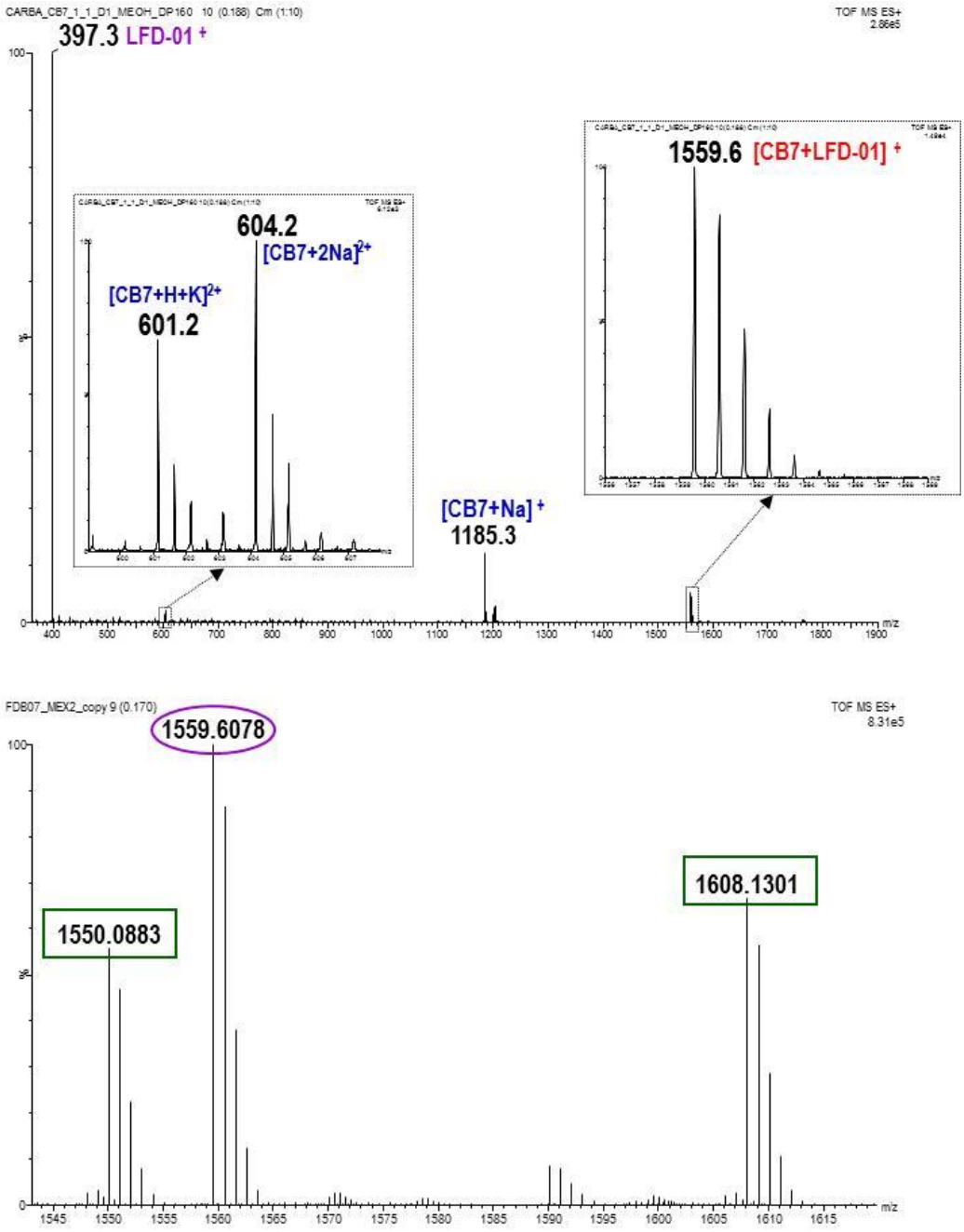

Figure S25. ESI-MS (top) and HRMS (bottom) spectra of LFD-**01** (0.1 mM) with CB[7] (1 mM) in water after a 1/10th dilution in a 0.1 mM methanolic solution.

Table S3. Accurate mass measurements for the ion at *m/z* 1559.6 assigned to [CB7+LFD-**01**]$^{1+}$ after internal calibration with two doubly charged PEG adducts at *m/z* 1550.0883 and *m/z* 1608.1301.

		m/z	error (mDa)	error (ppm)
Theoretical value		1559.6074	-	-
Experimental values	1	1559.6079	+ 0.5	+ 0.3
	2	1559.6078	+ 0.4	+ 0.3
	3	1559.6079	+ 0.5	+ 0.3
The experimental values are associated with an ion of elemental composition $C_{70}H_{75}N_{30}O_{14}^{+}$.				

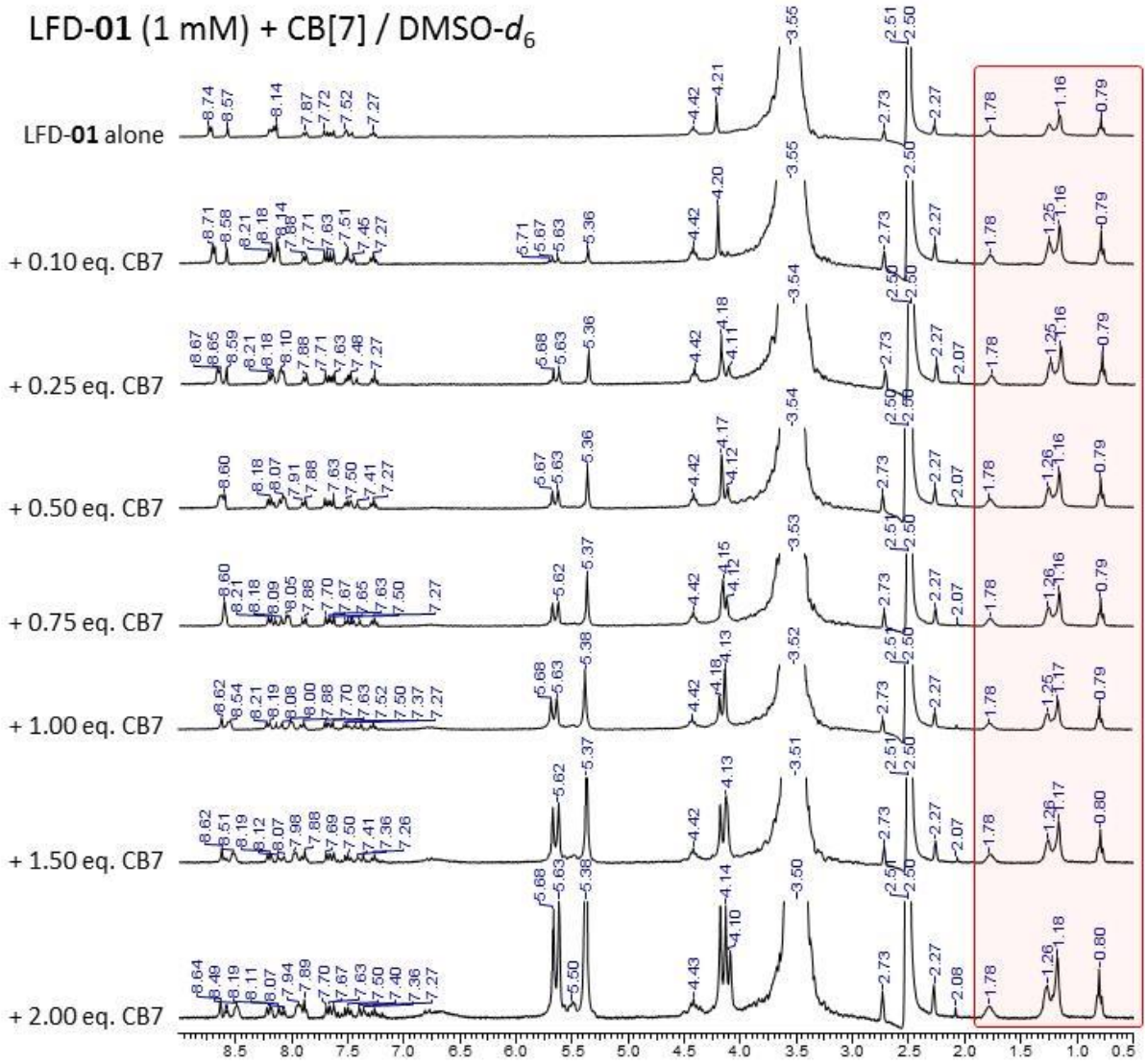

Figure S26. ^{1}H NMR titration of LFD-**01** with CB[7] in DMSO-d_6.

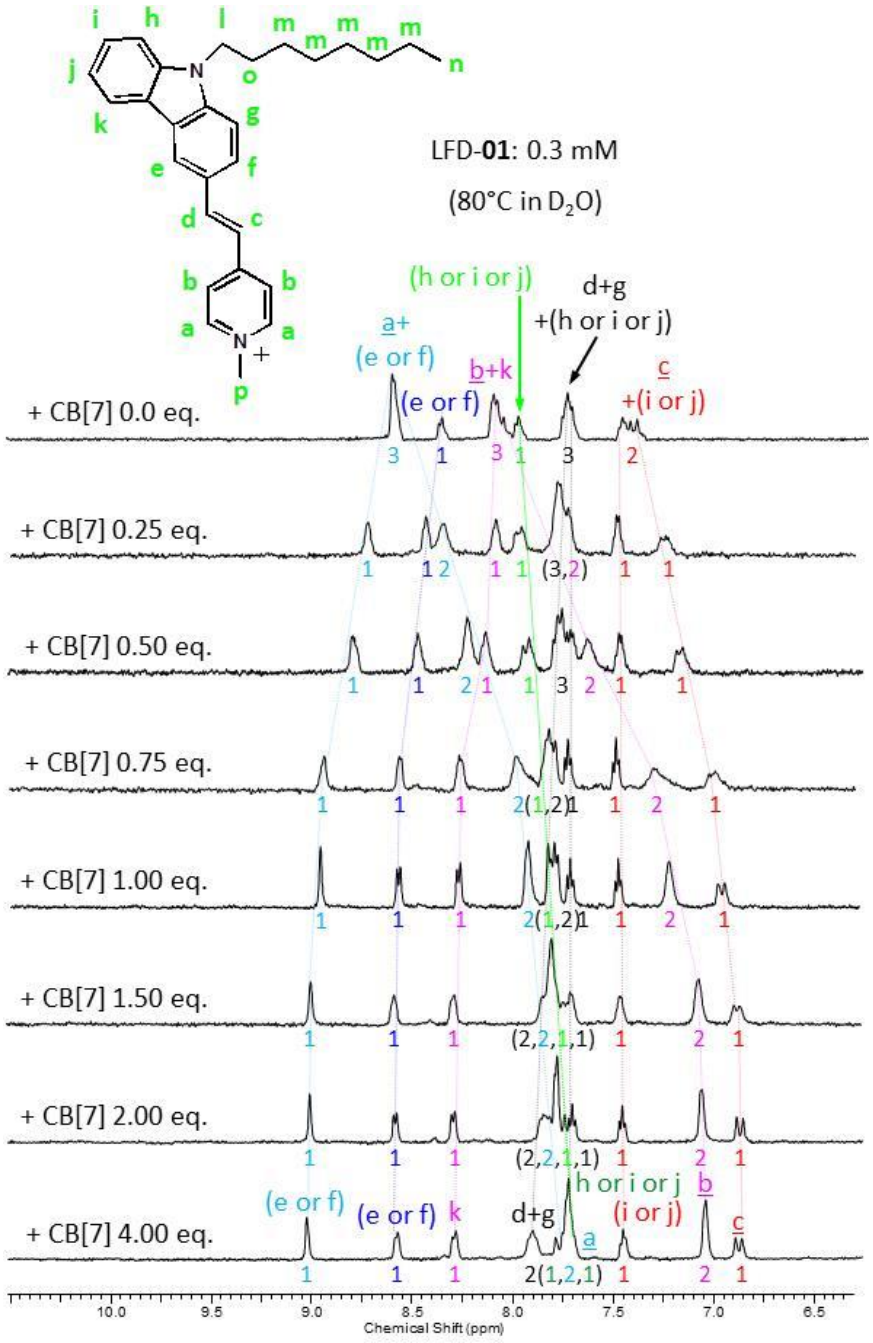

Figure S27. ^{1}H NMR titration of LFD-**01** with CB[7] in D_2O at 80°C (approximate values of signals integrals are given as colored numbers and help to the protons assignment).

Due to severe overlap of several signals, we could not assign all proton resonances. However, we relied on the COSY H-H spectrum (see Supplementary Fig. 28) and from the titration of Supplementary Fig. 25 (also using signal integrals which were very good) to propose a partial assignment. The purpose was to identify protons a, b and c which are supposed to be the most affected by CB[7] complexation. Based on signals positions and integrals within the titration and on the COSY H-H spectrum, we found three signals which moved significantly upfield (assigned to protons a, b and c), in line with what found in DMSO-d_6 (see Fig. 5 of the paper) and for the analogous compound LFD-**02** in D_2O (see Supplementary Fig. 29) and in DMSO-d_6 (see Supplementary Fig. S30).

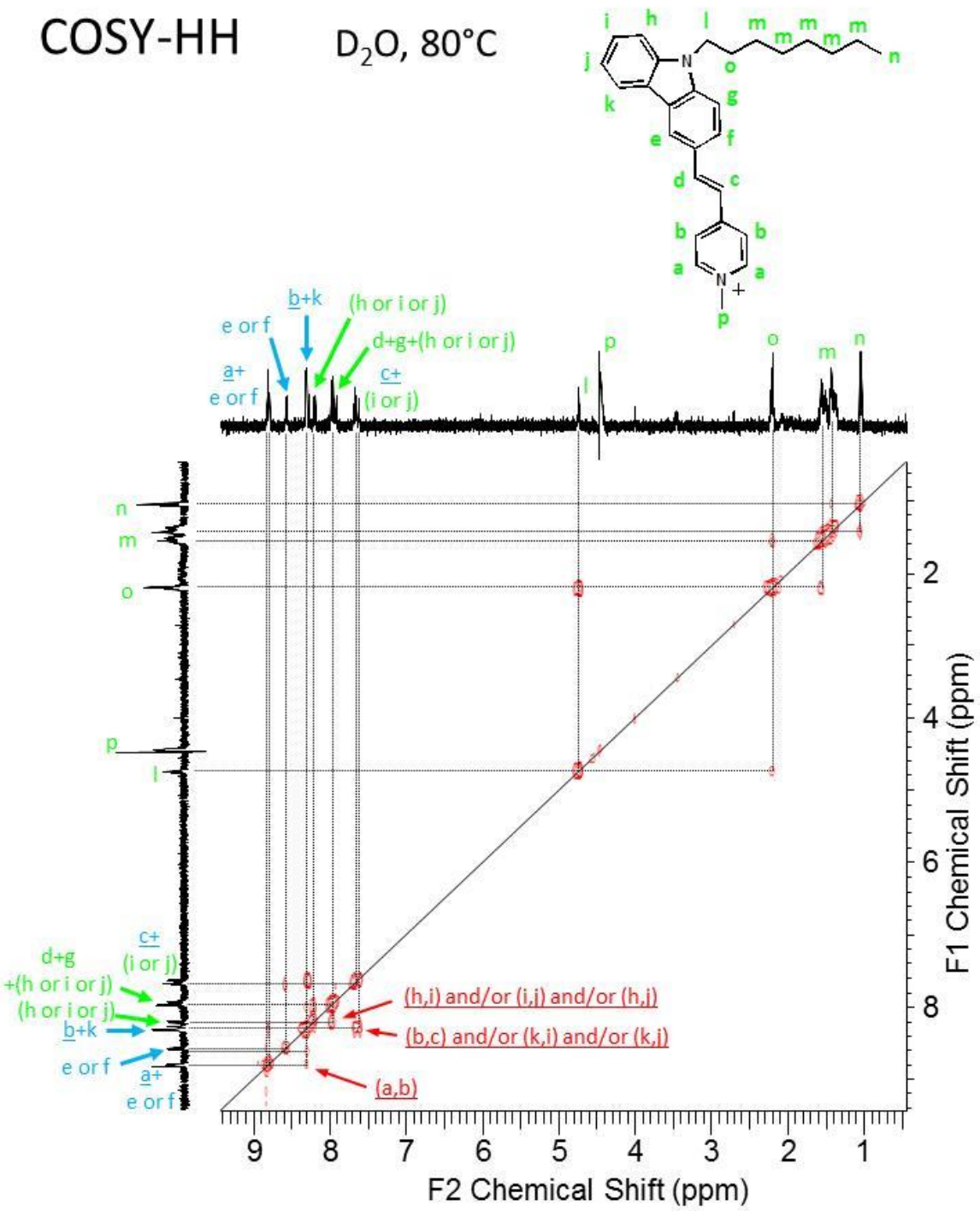

Figure S28. COSY H-H NMR spectrum of LFD-**01** (1 mM) in D_2O at 80°C.

The COSY NMR spectrum was recorded with a Bruker Avance 500 MHz Ultrashield NMR spectrometer with a Triple Broadband Inverse probe (TBI) at 353K. Chemical shifts are given in ppm relative to the residual peak of D_2O (δ = 4.70 ppm). The sequence corresponds to Bruker pulse program cosygpprqf using pulsed gradient and presaturation during relaxation delay. The SW was 20 ppm, the recovery delay of 1s and 16 scans were set for acquisition (P1=9 µs and Pl1=-3 dB).

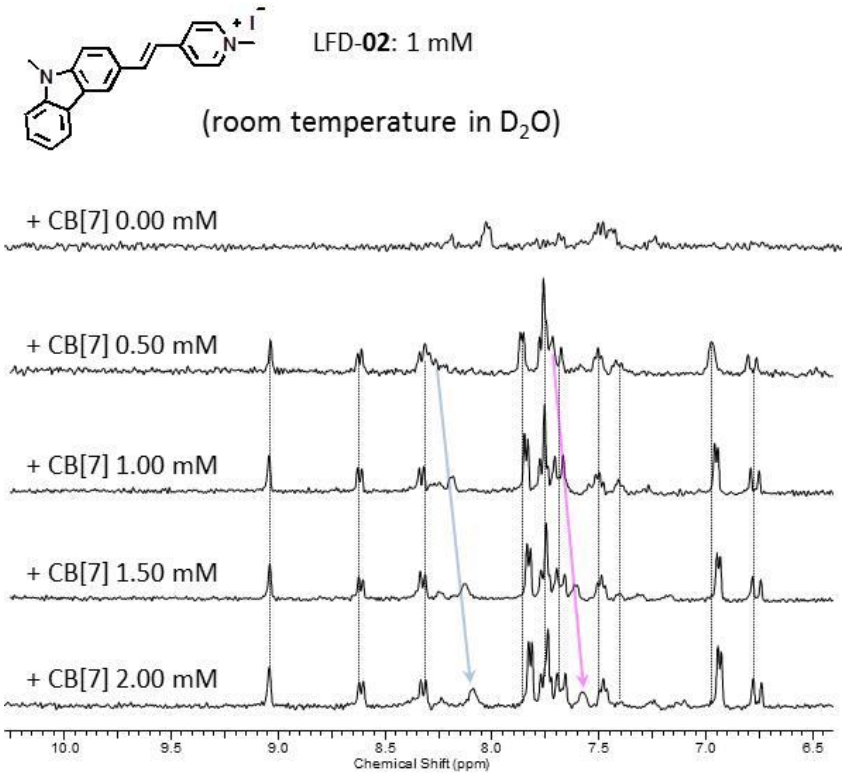

Figure S29. ^{1}H NMR titration of LFD-**02** with CB[7] in D_2O at room temperature.

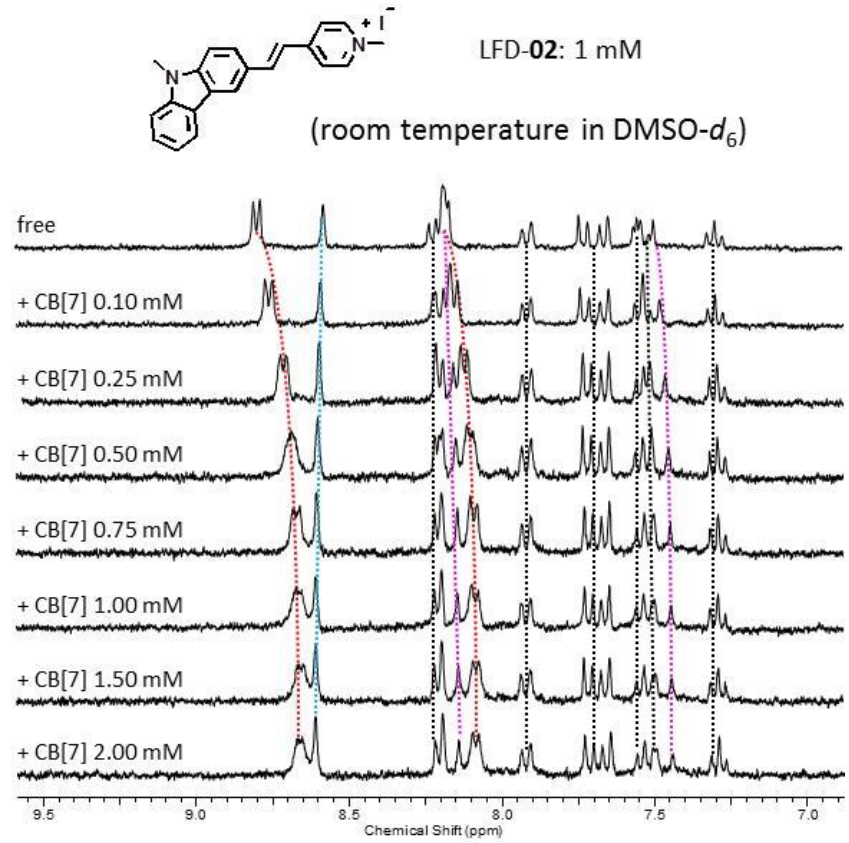

Figure S30. ^{1}H NMR titration of LFD-**02** with CB[7] in DMSO-d_6 at room temperature.

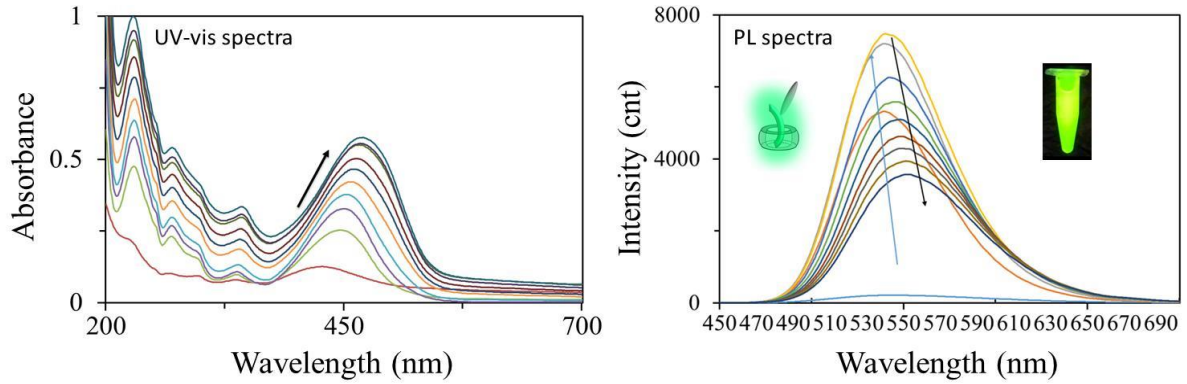

Figure S31. UV and PL titrations of LFD-**01** (20 μm) with CB[6] (120 μm) in water.

With CB[6], the main absorption peak is increased and red-shifted by ≈ 42 nm similar to what observed in organic solvents. The fluorescence is slightly blue-shifted when approaching equivalence before being red-shifted by ≈ 9 nm with respect to free LFD-**01** after adding more CB[6]. Estimate of the binding constant is: $K_a \approx 1.5 \times 10^5\ M^{-1}$. The quantum yield Φ_f = 0.734 has considerably increased at the equivalence point where the fluorescence is maximum. Job plots as determined by UV-vis titrations support a 1:1 CB[6]: LFD-**01** stoichiometry. The MS spectrum of an equimolar mixture of LFD-**01** and CB[6] (0.1 mM) in water showed peaks assigned to the host and guest and a new peak ascribed to a 1:1 complex that is confirmed by HRMS analyses for a peak at *m/z* 1393.5586 corresponding to the formulae $C_{64}H_{69}N_{26}O_{12}^{+}$ in line with the composition $[(\text{LFD-}\mathbf{01})(\text{CB6})]^{1+}$ (error < 1 ppm). However, we can not completely rule out the formation of 1:2 complexes.

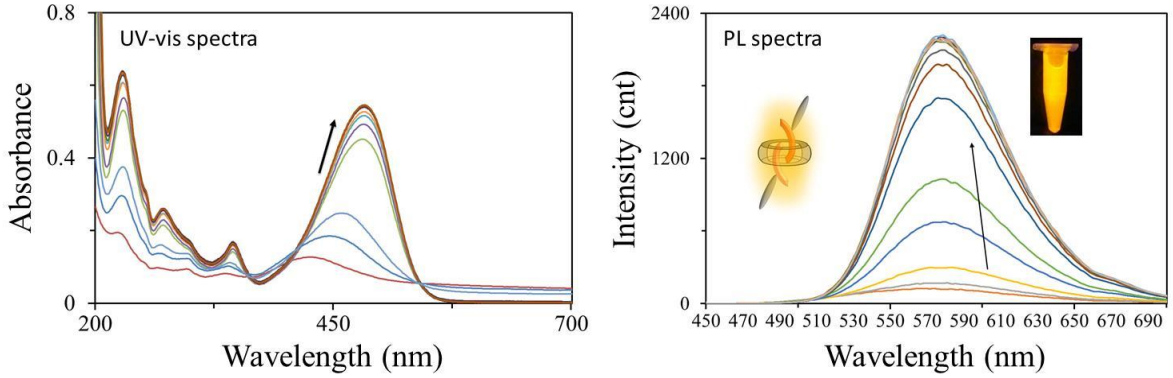

Figure S32. UV and PL titrations of LFD-**01** (20 μm) with CB[8] (120 μm) in water.

Concerning CB[8], recent works have shown that monocationic pyridinium compounds could be doubly accommodated so that a 1:2 stoichiometry is expected with two LFD-**01** guests included in one CB[8]. The absorbance of LFD-**01** is strongly increased in the presence of CB[8] and red-shifted by 61 nm, which is closely related to the trend observed in organic solvents. The fluorescence is shifted by ≈ 16 nm with respect to free LFD-**01** and again strongly increased (Φ_f = 0.338) but approximately half of the value observed for CB[6] or CB[7] binding. This smaller enhancement in fluorescence as compared to CB[6] and CB[7] may be due to self-quenching if we consider two guests per CB8. Job plots as determined by UV-vis titrations support a 1:2 CB[8]:LFD-**01** stoichiometry. HRMS allowed to characterize $(\text{LFD-}\mathbf{01})_1$@CB[8] and $(\text{LFD-}\mathbf{01})_2$@CB[8] complexes whereas $(\text{LFD-}\mathbf{01})_1$@$\text{CB[8]}_2$ species are hardly detected as trace amounts.

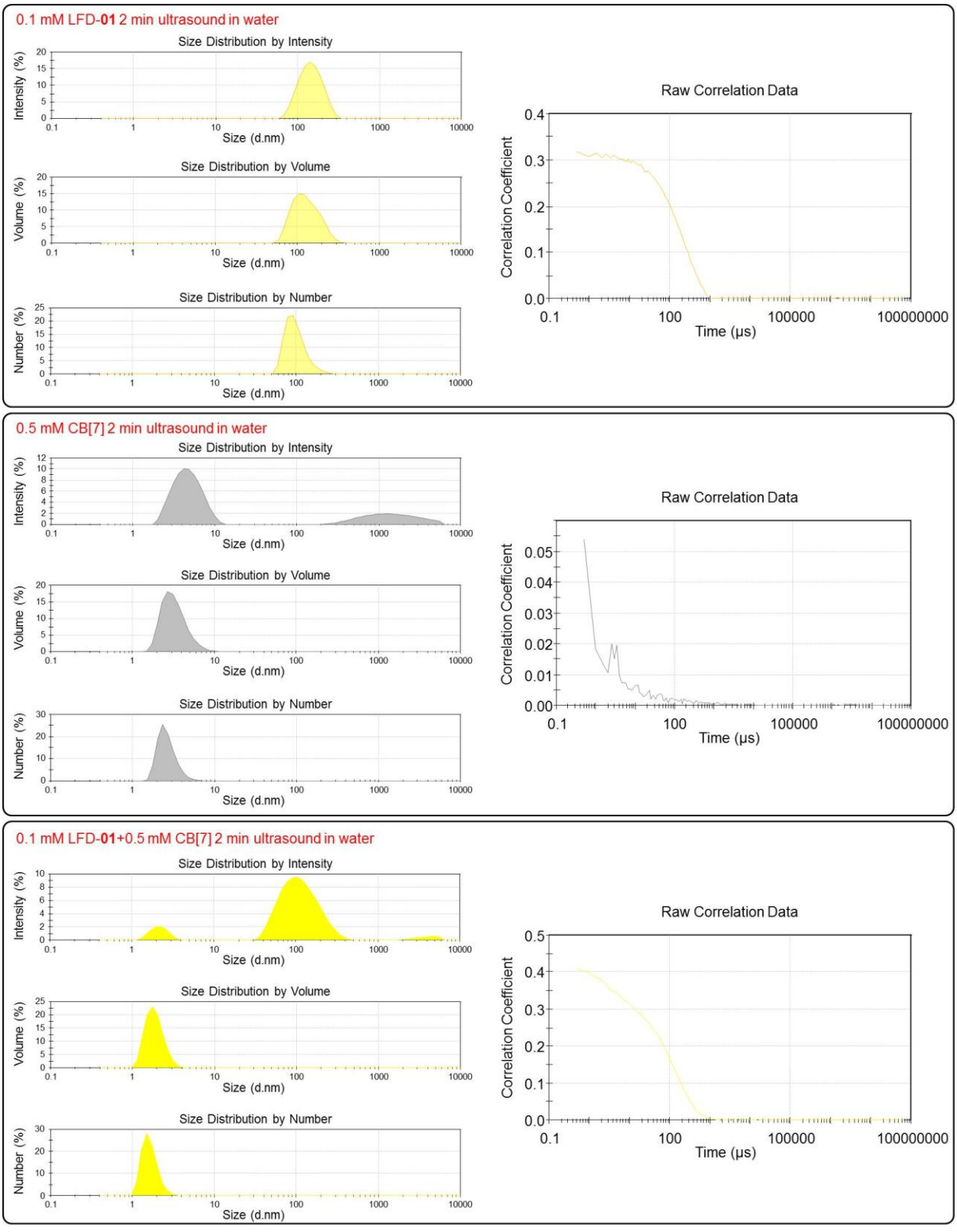

Figure S33. DLS of LFD-**01** alone, CB[7] alone and of a mixture of LFD-**01** and CB[7].

The final concentration of LFD-**01** and LFD-**02** was fixed to 0.1 mM. As can be seen in Supplementary Fig. 33, when CB[7] (0.5 mM) was added to LFD-**01** (0.1 mM), the particles size observed decreased to ≈ 2 nm which is close to the value expected for a 1:1 LFD-**01**:CB[7] complex. The results are clear when considering size distributions by volume and by numbers. As for intensity, the presence of another population of particles in the 30-300

nm window indicates that not all particles have disassembled. This is probably because at these particular concentrations (0.1 mM guest, 0.5 mM host) and for the reported binding constant, about 90% of LFD-**01** is complexed which leaves a portion of the guest free, so prone to be found as nanoparticles. The high intensity of the profile at 30-300 nm likely reflects the very strong dependence of the intensity of light scattered, with respect to the particles diameter. Indeed, for example, a 100 nm particle will scatter one million times as much light as a 10 nm particle and for this reason, the size distribution given by intensity, which is the more direct measurement and often the most relevant, has to be taken with care. Results are very similar when using CB[7] at 0.1 mM and at 3.0 mM concentrations. LFD-**02** has comparable profiles (intensity, volume and number) with respect to those of LFD-**01**. The tripeptide Gly-Gly-Gly has been used as a control in addition of CB[7] as probes for small size particle determination (isolated molecules). Although the usual polystyrene latex model worked fine in all cases, we had to change the model to get data that could be measured for CB[7] and for Gly-Gly-Gly. The only one working was the cellulose acetate g_PS model (RI: 0.1 and Absorption: 0.1) and we got distribution profiles for Gly-Gly-Gly (intensity [range 1-20 nm], volume [range 0.6-6 nm] and number [range 0.6-3 nm]) in agreement with isolated or loosely aggregated molecules. The data for CB[7] are shown in Supplementary Fig. 33.

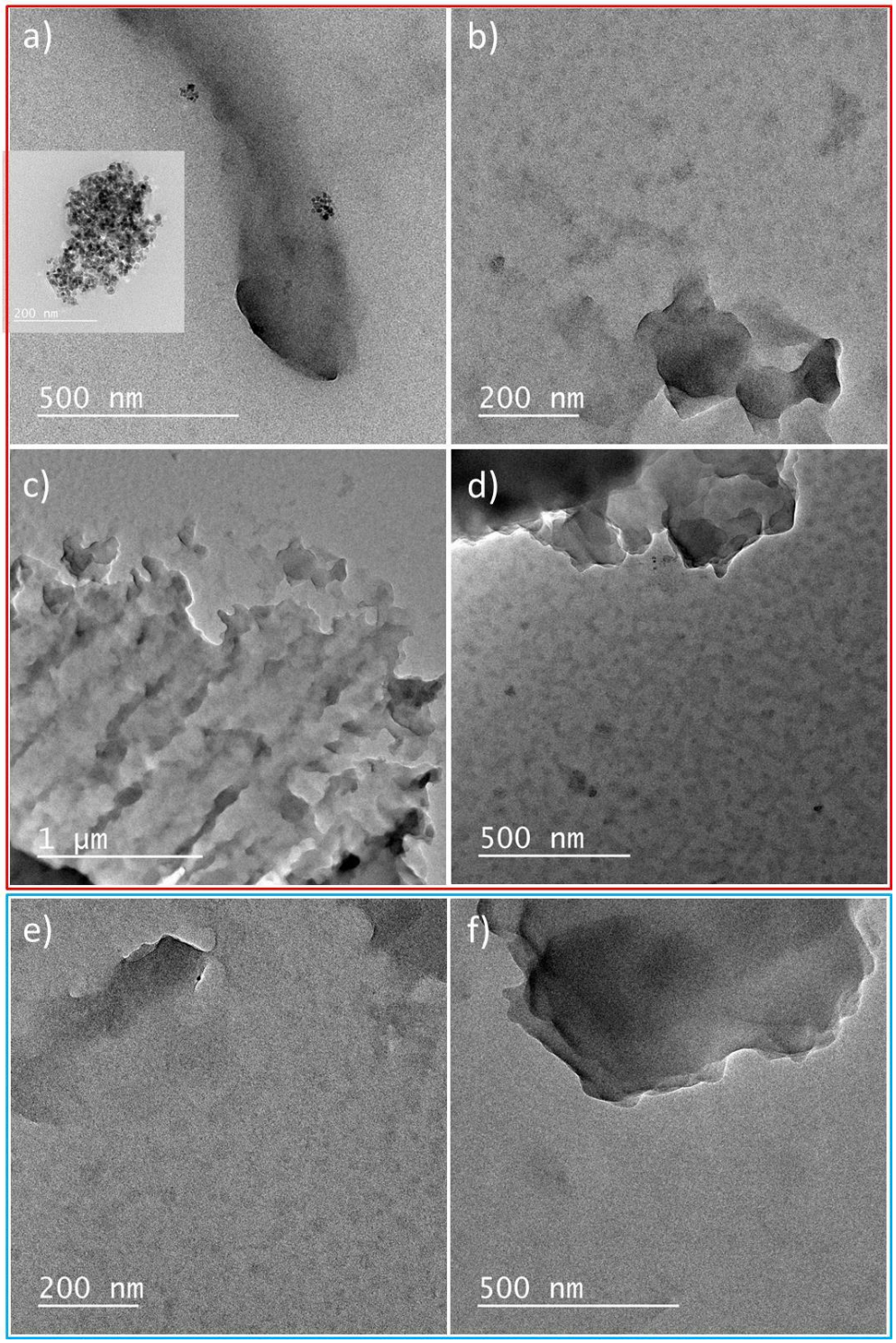

Figure S34. TEM images of LFD-**01** (0.1 mM) with CB[7] [a (0.1 mM), b, c, d (0.6 mM)] and of LFD-**02** (0.1 mM) with CB[7] [e (0.1 mM) and f (0.6 mM)].

We still noted the presence of nanoparticles for equimolar amounts of CB[7] but as the concentration increased, we observed an almost disappearance of the previously characterized nanoparticles (see Fig. 3d of the paper). This is also clear in the case of LFD-**02**. Moreover, amorphous films ascribed to CB[7] (which is known to give amorphous powders) can be seen (b, c, d, f) when excess CB[7] was used. These images are in good agreement with the DLS results of Supplementary Fig. 33.

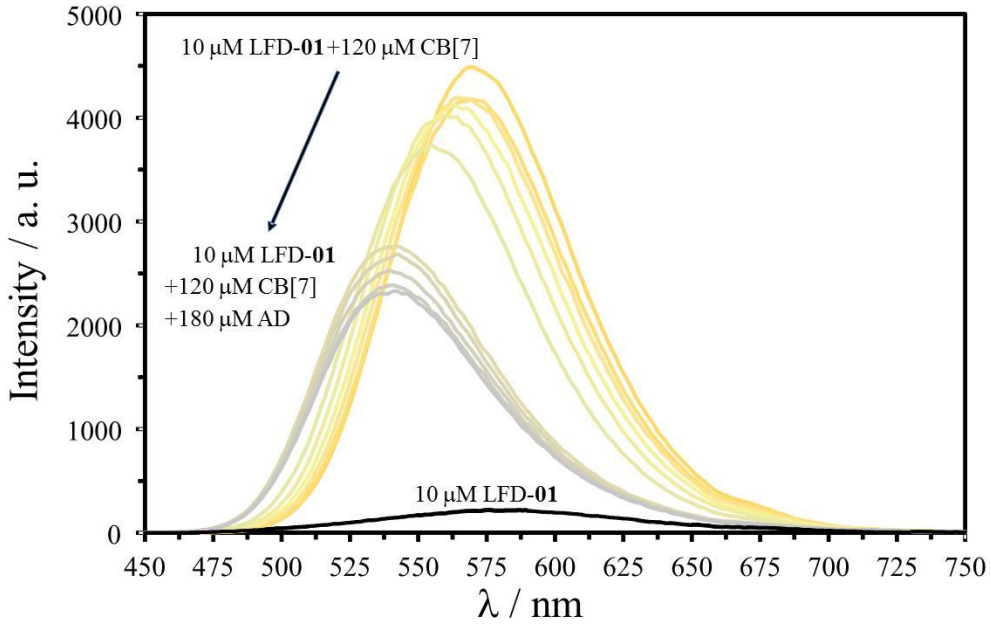

Figure S35. Competition experiments with a growing concentration of amantadine toward inclusion in CB[7] (K_a = $10^{12.6}$ M^{-1}). As expected, LFD-01 is aggregated in water and has its fluorescence quenched. Upon CB[7] addition, the fluorescence increased to the maximum shown here. After addition of amantadine which has a better affinity toward CB[7], amantadine is complexed and expell LFD-01 out of the cavity resulting in fluorescence decrease.

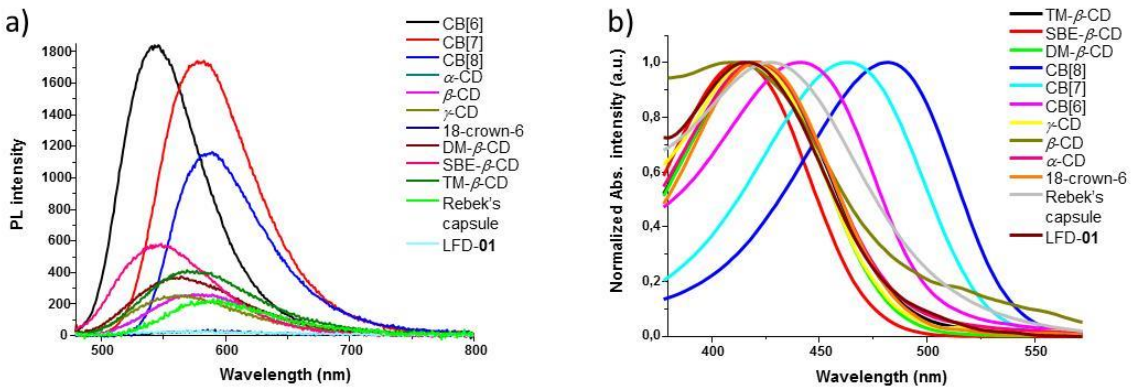

c)

Host	Concentration	Φ_f	λ_{exc}	λ_{em}	max abs.
CB[6]	20 µM	0.734	450 nm	544 nm	440
CB[7]	800 µM	0.597	460 nm	580 nm	463
CB[8]	40 µM	0.338	460 nm	588 nm	481
α-CD	4 mM	0.140	450 nm	572 nm	420
β-CD	2 mM	0.170	440 nm	578 nm	410
γ-CD	8 mM	0.245	450 nm	562 nm	420
18-crown-6	8 mM	0.025	440 nm	585 nm	420
DM-β-CD	8 mM	0.237	460 nm	560 nm	420
SBE-β-CD	8 mM	0.289	460 nm	578 nm	413
TM-β-CD	8 mM	0.195	460 nm	573 nm	420
LFD-**01**	20 µM	0.021	420 nm	572 nm	415
Rebek's capsule	2 mM	0.049	470 nm	586 nm	427

Figure S36. Screening of the presence of macrocycles by LFD-**01** (fixed concentration of 20 µM) in water as monitored by PL spectra in a) and normalized UV spectra in b) followed by a table summarizing host concentrations, quantum yields, excitation and emission wavelenghts and the maximum absorbance.

This approach allows for rapidly assessing the presence of a macrocycle in water. Even if this approach may appear limited due to the design of the dye, containing an alkyl chain and a pyridinium head, this screening shows that some of the most popular macrocycles are being recognized by LFD-**01**,excepted 18-crown-6 (dark blue trace behind that of LFD-**01**, Fig. S36a). Measurements were performed by preparing a stock aqueous solution of LFD-**01** at 100 µM subsequently mixed with the relevant macrocycles affording 0.5 mL solutions before 1/5th dilution for filling the cells (2.5 mL final volumes, final concentrations are given in the Table of Fig. S36c).

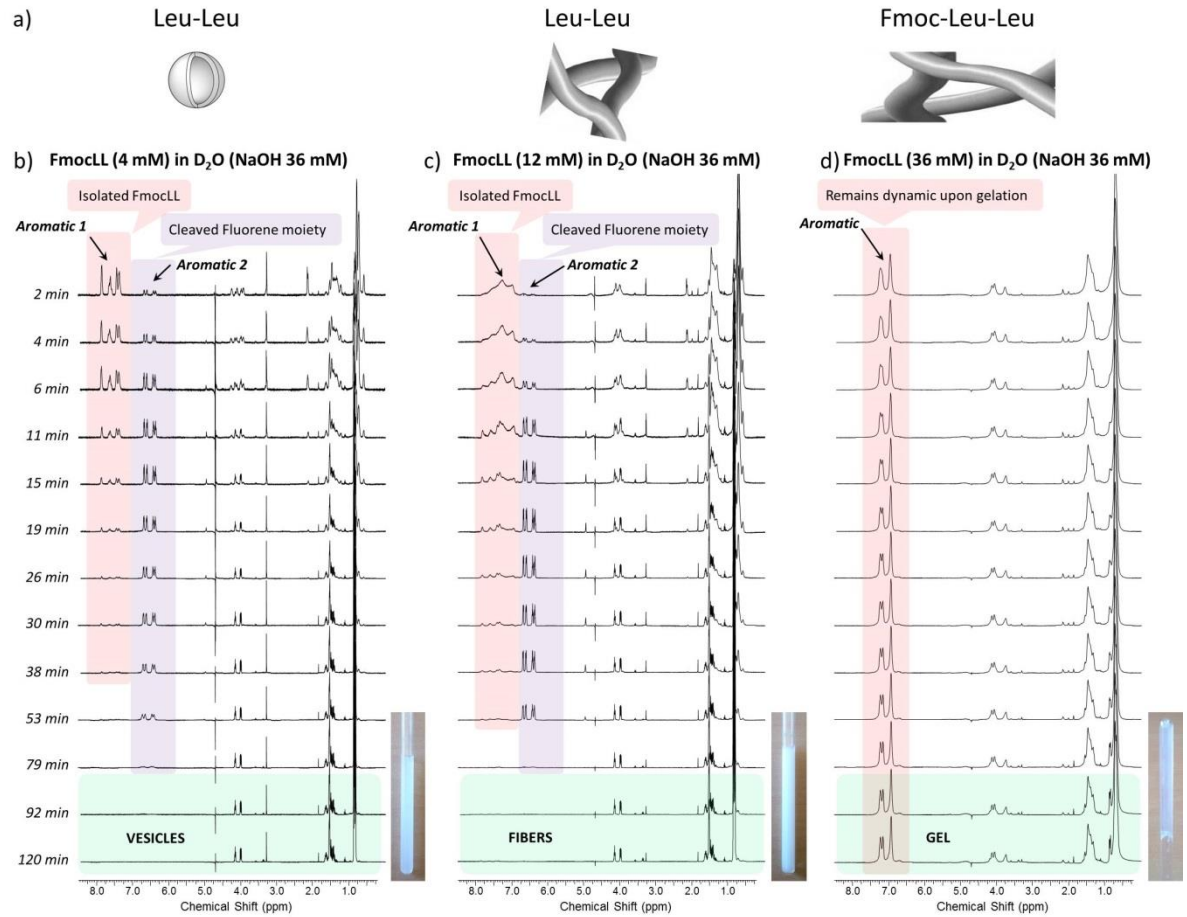

Figure S37. Kinetics of vesicle, fibers and gel formation a) starting from Fmoc-Leu-Leu as monitored by ^{1}H NMR in D_2O at (b) 4 mM (Leu-Leu), (c) 12 mM (Leu-Leu) and (d) 36 mM (Fmoc-Leu-Leu; fixed starting concentration in NaOH = 36 mM).

At 36 mM, the p*H* is close to 8-9 (Fmoc still linked to Leu-Leu) while at 4 and 12 mM Fmoc-Leu-Leu, p*H* is above 10 thus increasing the likelyhood of Fmoc cleavage (see above, Supplementary Fig. 37) and Leu-Leu vesicle formation.

Controls at 4 mM Fmoc-Leu-Leu and 4 mM NaOH show only minor modifications of the ^{1}H NMR spectrum with time over 2 hours. 2D-NOESY spectra show cross correlations between the aromatic section and the rest of the spectrum that have the same sign as that of the diagonal suggesting aggregation in agreement with what found at 36 mM (see Supplementary Fig. 41). The cross peaks are hardly visible (32 scans) at 150 ms mixing time and much better seen as the mixing time increases with the best case at 800 ms of mixing time. However, we did not observe gel formation at this concentration.

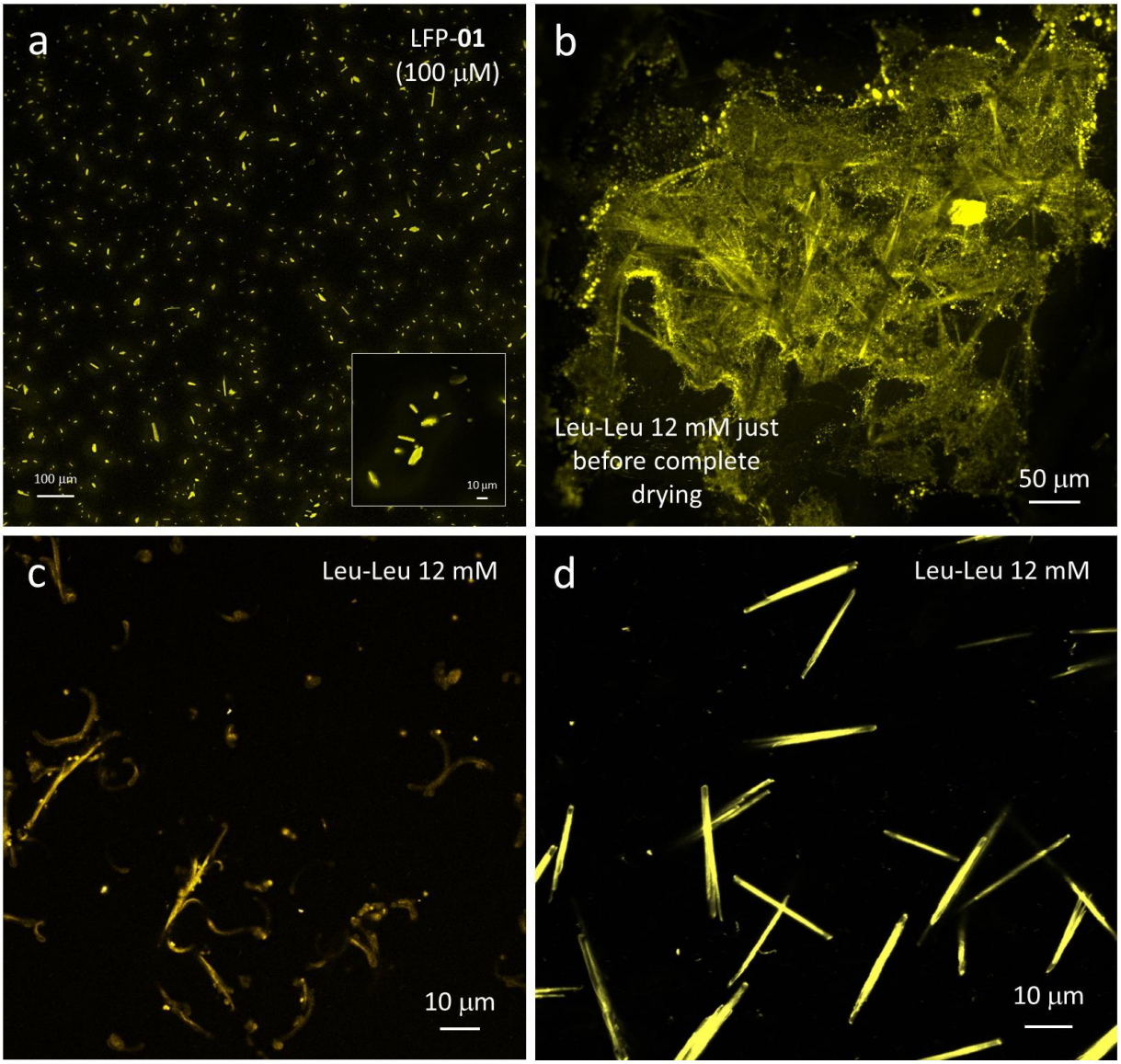

Figure S38. Confocal microscopy image of suspensions of (a) LFP-**01** after ultrasound exposure for 2 minutes (brightly seen due to the sensitivity of the microscope even if the fluorescence of LFD-**01** alone is low in water), (b) Leu-Leu (12 mM) just before complete drying, (c) and (d) Leu-Leu (12 mM).

The structures in Supplementary Figure 38a are assigned to amorphous LFP-**01** particles (obtained after ultrasound exposure at 0.1 mM for 2 minutes). Samples of LFP-**01** particles obtained after dilution to 50 μM from a stock solution at 2.5 mM exposed to ultrasound for 10 minutes (standard for alginate experiments) showed almost identical objects. The structures in Supplementary Figure 38d could be assigned to Leu-Leu microtubes due to the darker contrast on the extremities.[13]

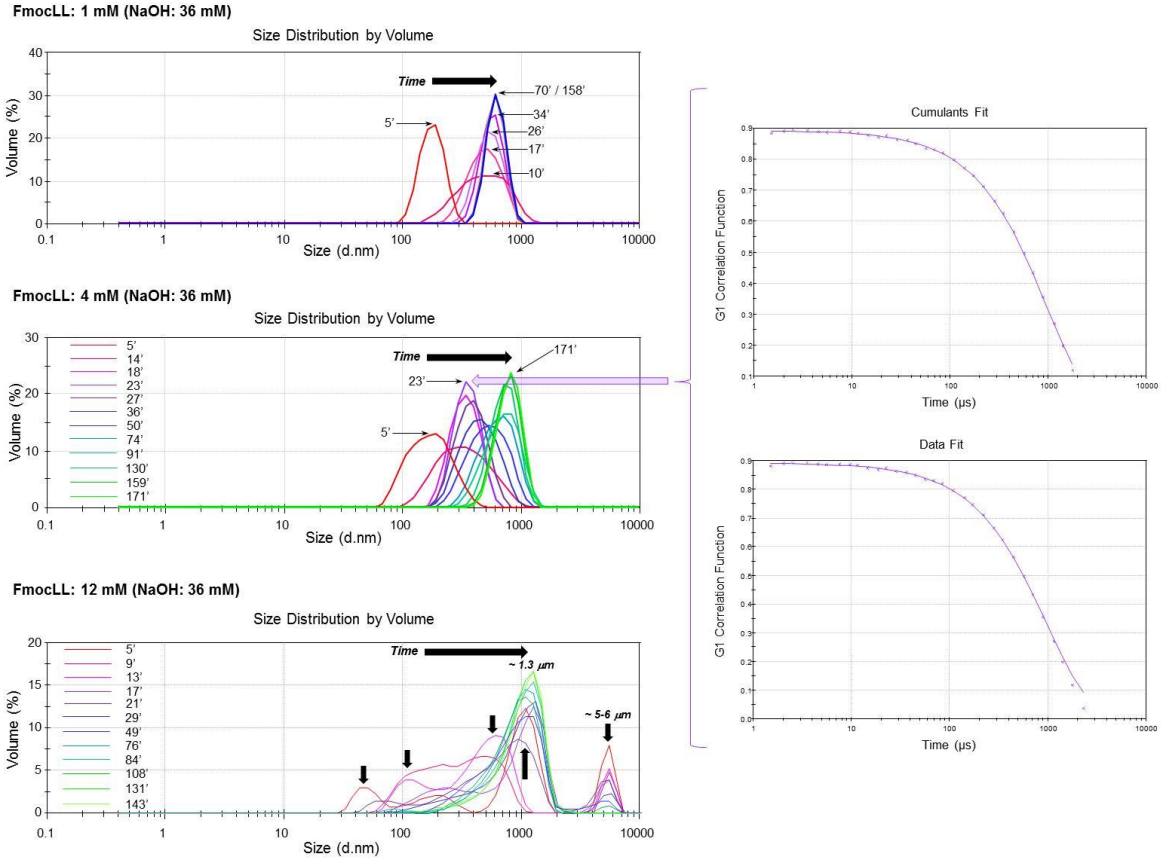

Figure S39. DLS of Fmoc-Leu-Leu at 1, 4, and 12 mM in water ([NaOH]=36 mM). At basic p*H*, Leu-Leu vesicles formed at 1 and 4 mM and fibers at 12 mM of starting material, see text of the paper.

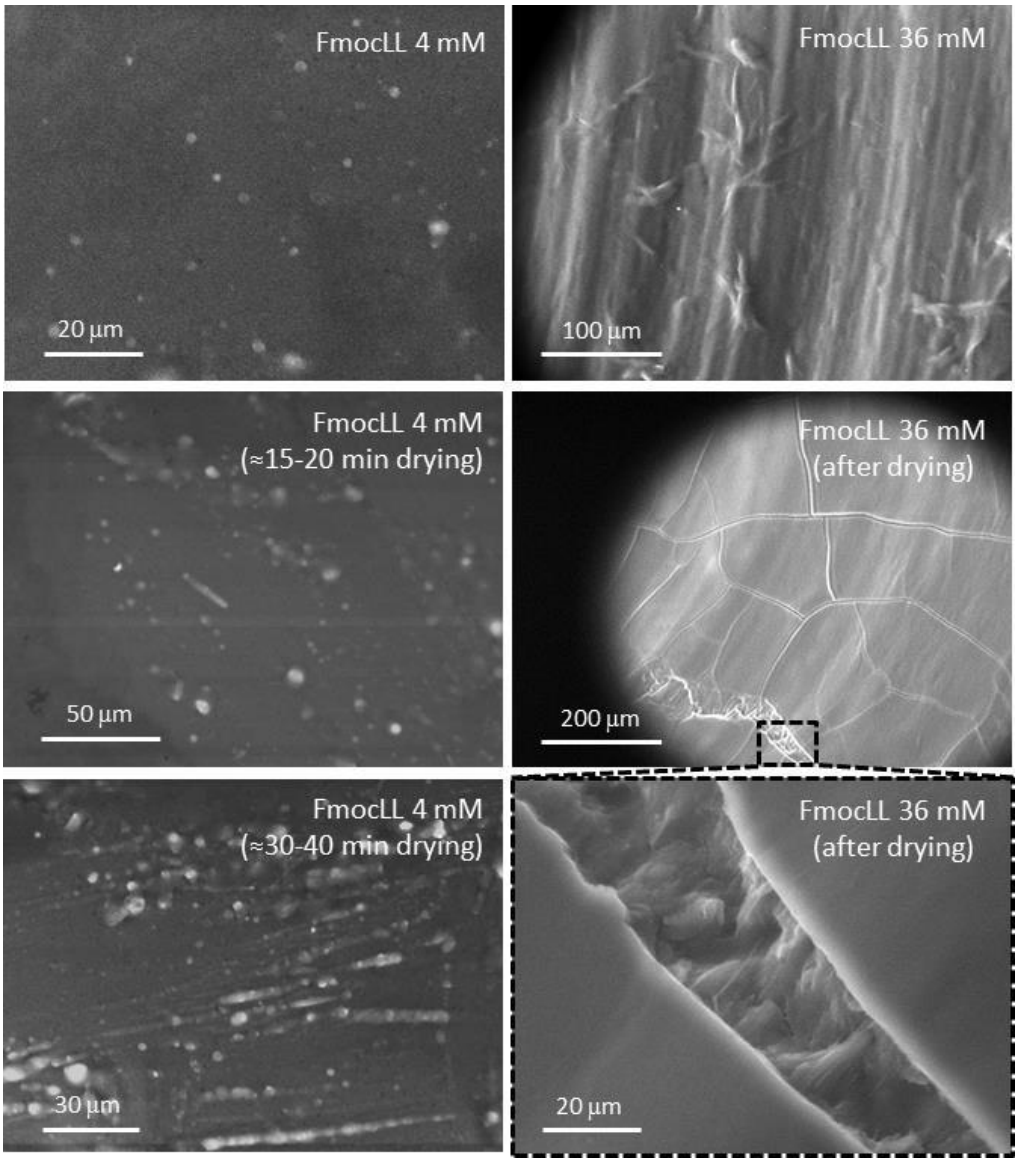

Figure S40. Environmental SEM of Fmoc-Leu-Leu (4 and 36 mM) in water ([NaOH]=36 mM). Leu-Leu vesicles formed at 4 mM and fibers at 36 mM of starting material, see text of the paper. Note the spheres fusion as the compound is gradually dried over the surface at 4 mM. A film was seen by this technique at 36 mM concentration of Fmoc-Leu-Leu

Interestingly, samples at 12 and 36 mM dried using the environmental mode show the formation of supramolecular films as already reported for analogous compounds[14] but no fibers networks.

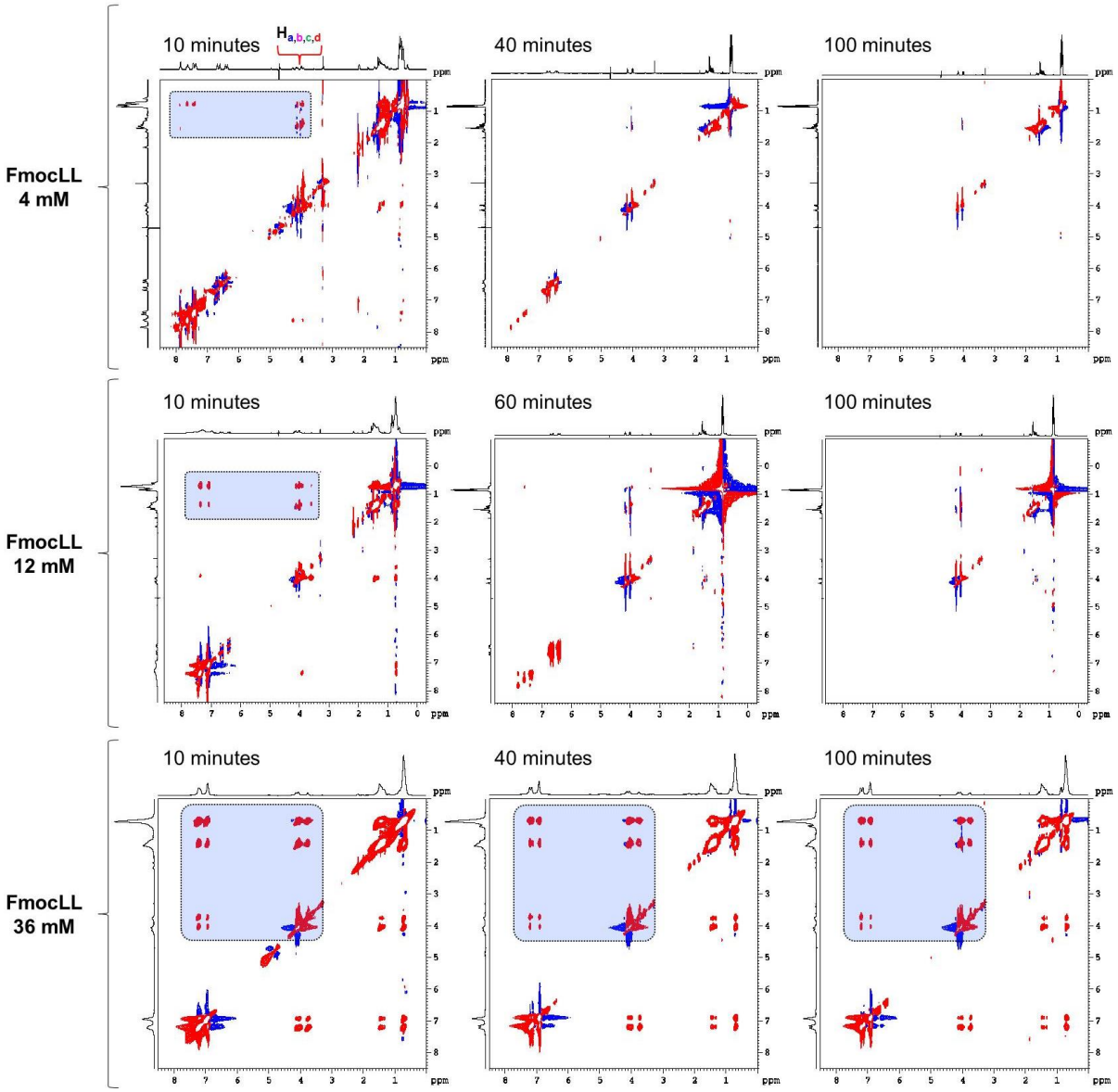

Figure S41. Kinetics of Fmoc-Leu-Leu deprotection at 4 and 12 mM and Fmoc-Leu-Leu aggregation at 36 mM as monitored by 2D-NOESY NMR in D_2O (room temperature, mixing time: 150 ms, starting [NaOH]=36 mM). Leu-Leu vesicles formed at 4 mM, Leu-Leu fibers at 12 mM and Fmoc-Leu-Leu fibers at 36 mM, see text of the paper.

At 36 mM, the p*H* is close to 8-9 while at 4 and 12 mM Fmoc-Leu-Leu, it is >10 thus increasing the likelyhood of Fmoc cleavage and Leu-Leu vesicle formation (see Supplementary Fig. 37). The 2D-NOESY NMR spectra were recorded with a Bruker Avance 500 MHz Ultrashield NMR spectrometer with a Double Resonance Broad Band Probe (BBFO) at 300K. The chemical shifts are given in ppm relative to the residual peak of D_2O (δ = 4.70 ppm). The sequence corresponds to Bruker pulse program noesyphpr phase sensitive with presaturation during relaxation delay and mixing time. The SW was 14 ppm, the recovery delay of 1s, the mixing time of 150 ms, and 2 scans were set allowing regular (each 10 minutes) acquisitions (P1 = 12 µs and Pl1 = -2 dB).

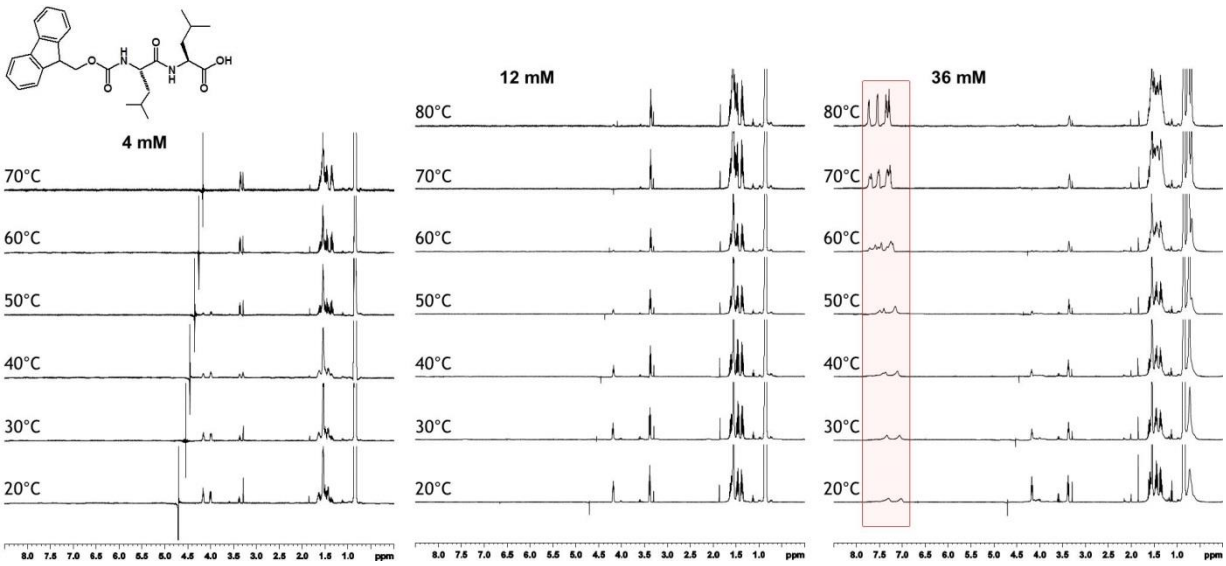

Figure S42. Variable temperature ^{1}H NMR spectra of Fmoc-Leu-Leu at 4, 12, and 36 mM (starting concentrations) in D_2O after vesicle and gel formation (initial [NaOH]=36 mM). Leu-Leu vesicles formed at 4 mM, Leu-Leu fibers at 12 mM, Fmoc-Leu-Leu fibers at 36 mM.

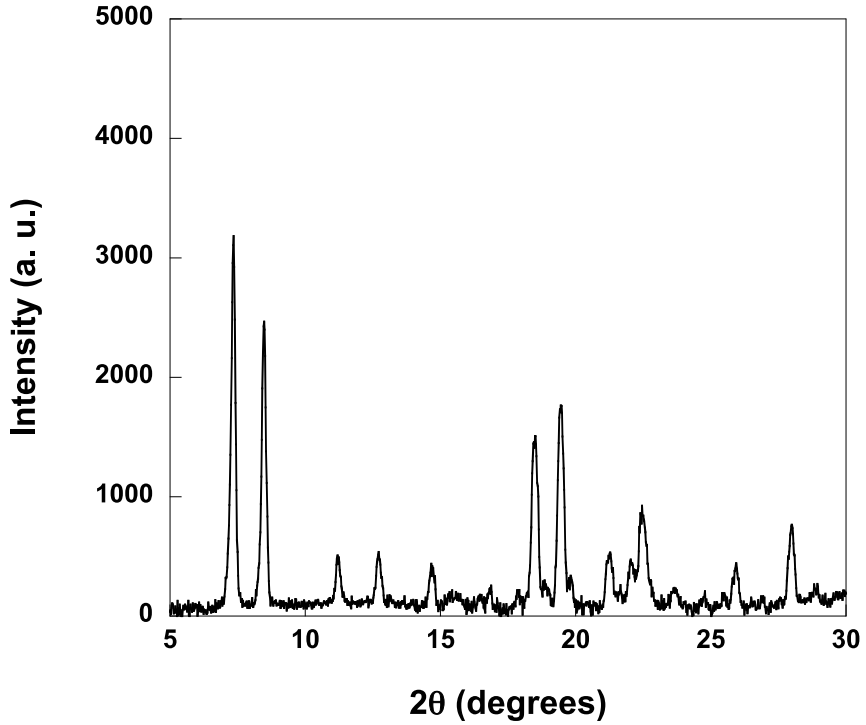

Figure S43. PXRD pattern of Phe-Phe material prepared exactly as for samples pictured in Figure 6d of the paper and in Figure S44.

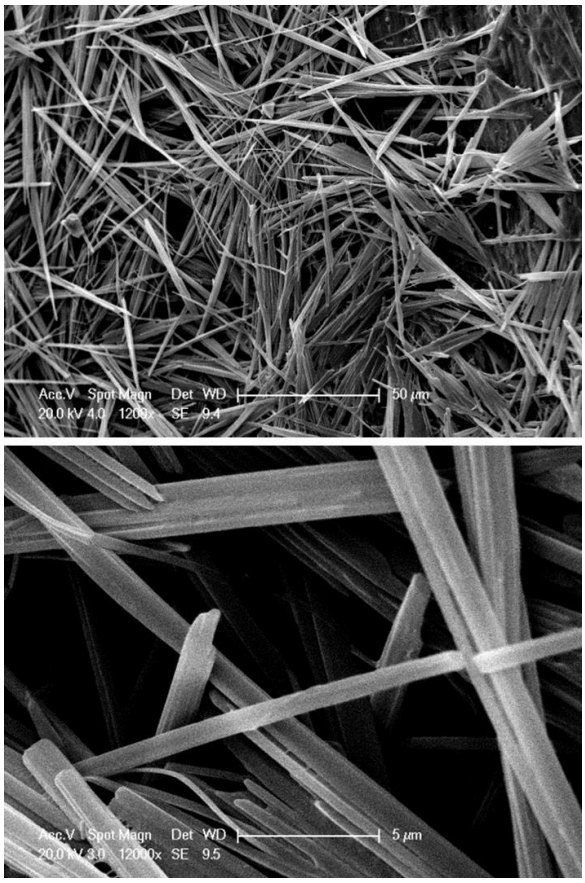

Figure S44. SEM of Phe-Phe dipeptide after solvent evaporation and gold staining.

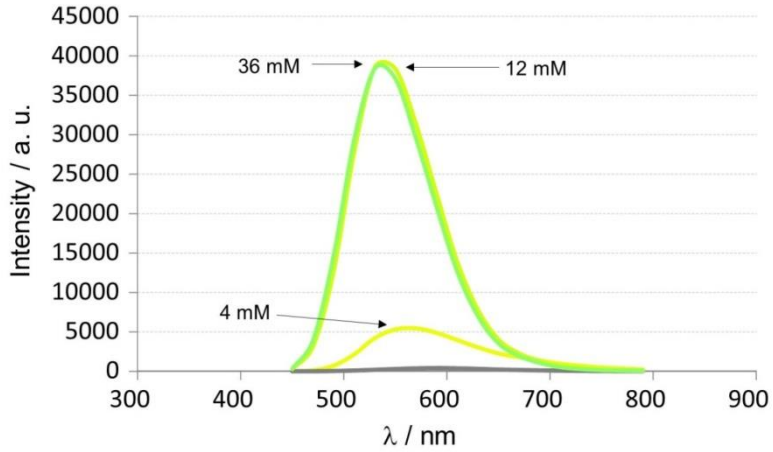

Figure S45. PL spectra of LFD-**01** (0.1 mM) with Fmoc-Leu-Leu at various concentrations (λ_{exc} = 420 nm) right after the addition of NaOH (36 mM) that initiates the self-assembly of Leu-Leu (4 and 12 mM) or Fmoc-Leu-Leu (36 mM). The minimum lag time allowing enough mixing and sample introduction in the machine before recording was 40 seconds. Grey trace = spectrum of LFD-**01** alone at 0.1 mM.

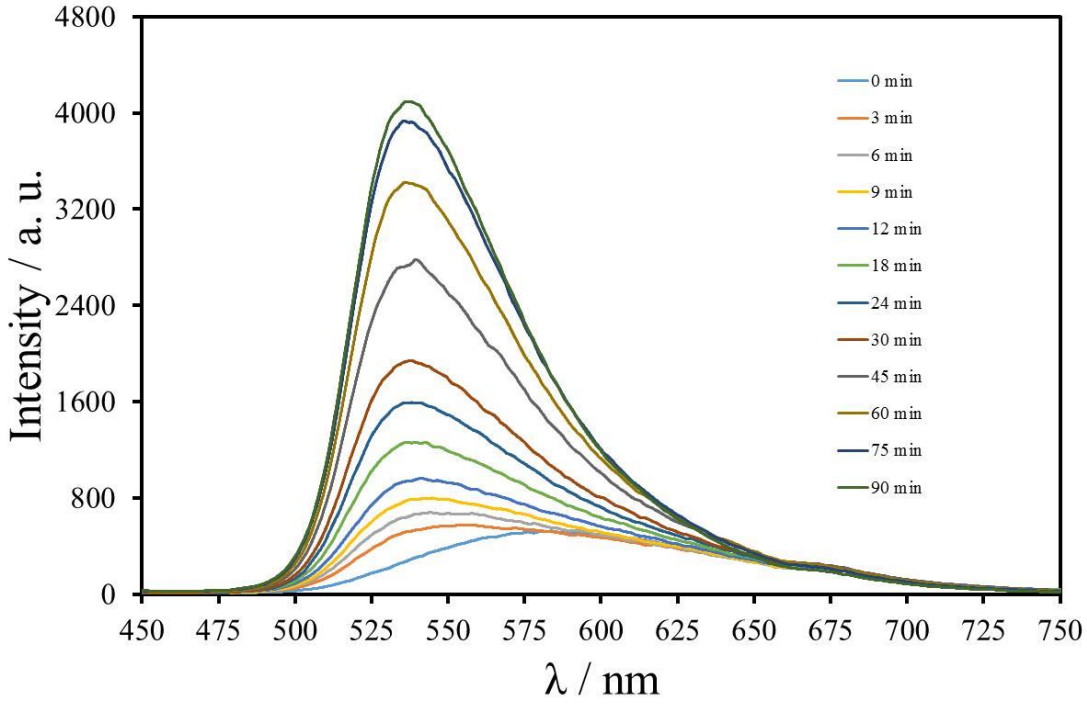

Figure S46. PL monitoring over time of alginate gelation (0.1% wgt) with 5% wgt Ca^{2+} ions using 50 μM LFP-**01** particles.

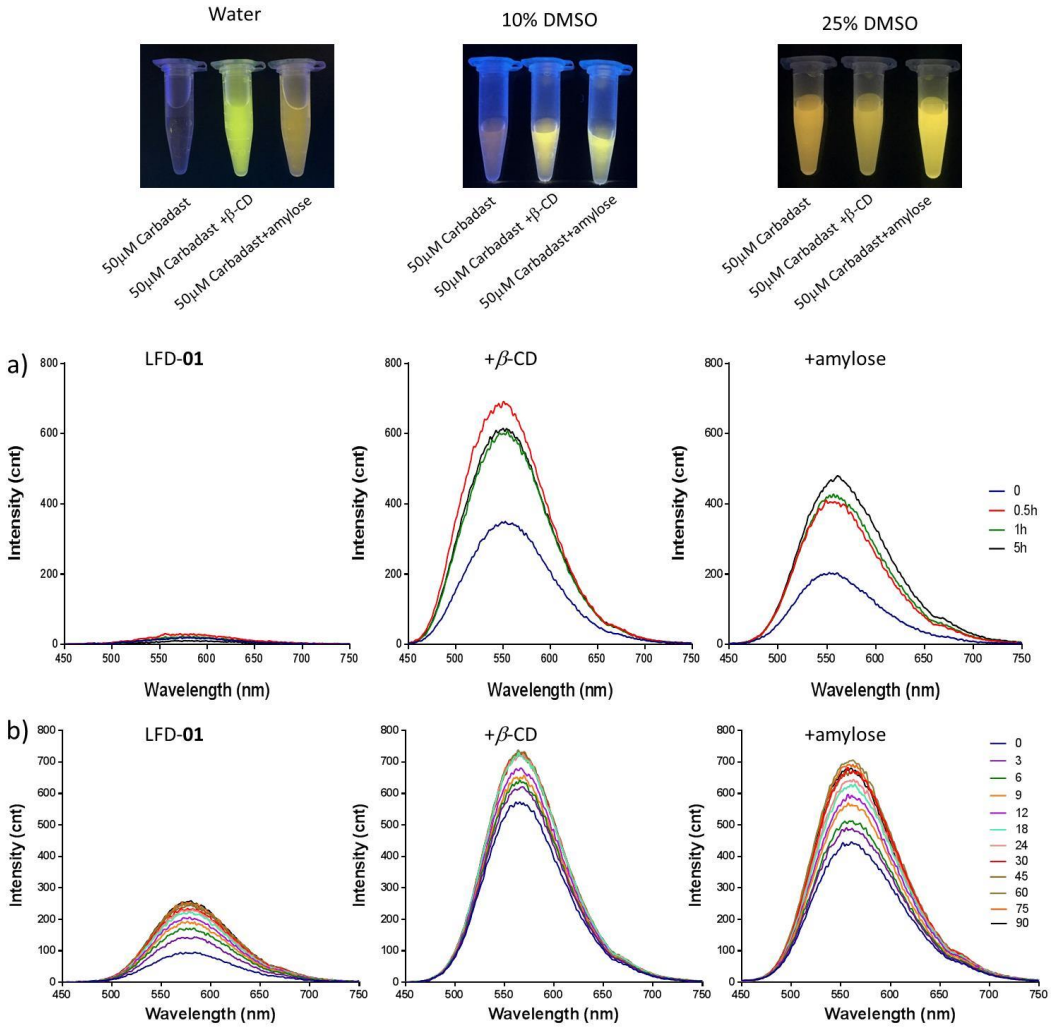

Figure S47. Fluorescence study of LFD-**01** (50 μM) with β-CD (2 mg/ml) and amylose (2 mg/mL) a) in water and b) in 10% DMSO.

Since amylose could not be well dissolved in water, its polymer chains may not unfold sufficiently and produce hydrophobic pockets for LFD-**01** dispersion. DMSO was then added to facilitate amylose dissolution. However, DMSO moderately solubilized LFD-**01** and we thus limited its percentage to 10.

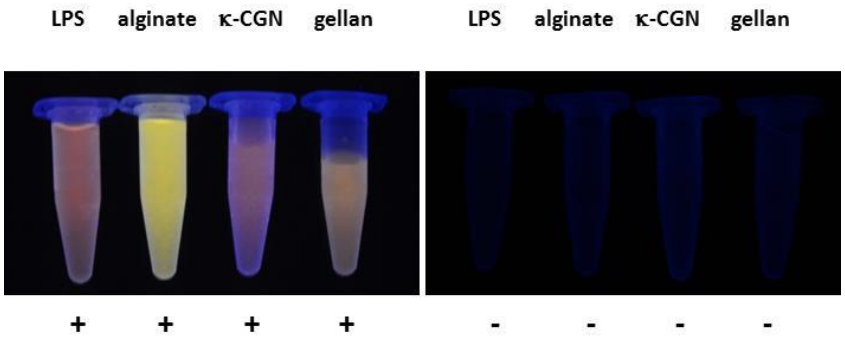

Figure S48. Fluorescence Turn-on of LFD-**01** (50 μM) with other polysaccharides (gellan, kappa-carrageenan, and a lipopolysaccharide).

LFD-01@CB[7] 1:1 complex, pyridinium side

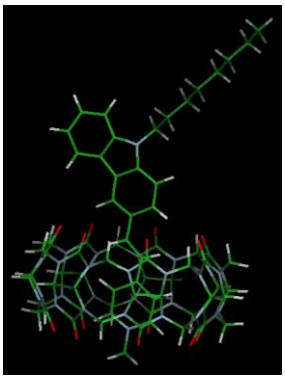

```
  189
scf done: -5408.667180
 N    -9.487445     2.811964     1.317416
 C   -10.851792     3.105886     1.351446
 C   -10.616028     0.865769     0.908291
 C    -9.332694     1.468447     1.042926
 C   -10.716693    -0.494993     0.639672
 C    -9.549719    -1.273251     0.501607
 C    -8.278432    -0.647212     0.643612
 C    -8.158278     0.707447     0.907503
 C   -12.883685     4.342136     1.580082
 C   -13.629335     3.172603     1.344419
 C   -12.989953     1.957334     1.108185
 C   -11.590544     1.918358     1.108170
 C   -11.489134     4.328366     1.586848
 C    -9.717731    -2.684212     0.214784
 C    -8.746416    -3.615074     0.010674
 C    -8.983897    -5.007386    -0.297672
 C   -10.262569    -5.617407    -0.354225
 C   -10.396058    -6.943728    -0.689634
 N    -9.311712    -7.711198    -0.976810
 C    -8.067091    -7.177060    -0.910170
 C    -7.884943    -5.855381    -0.572428
 C    -9.501928    -9.093202    -1.459490
 C    -8.414777     3.788408     1.482334
 C    -8.057062     4.530364     0.186202
 C    -6.957054     5.576302     0.405576
 C    -6.603553     6.357274    -0.867090
 C    -5.514575     7.415085    -0.646620
 C    -5.169680     8.212561    -1.911031
 C    -4.086026     9.275289    -1.687606
 C    -3.751509    10.072910    -2.952452
 H   -11.689040    -0.968204     0.534321
 H    -7.370993    -1.234711     0.547370
 H    -7.176543     1.159624     1.005304
 H   -13.403064     5.279324     1.759946
 H   -14.714474     3.220056     1.346842
 H   -13.565265     1.052529     0.929819
 H   -10.927599     5.239550     1.766836
 H   -10.758139    -2.997414     0.151685
 H    -7.700796    -3.320885     0.051017
 H   -11.165397    -5.060310    -0.137766
 H   -11.356464    -7.441881    -0.742683
 H    -7.239252    -7.833825    -1.147776
 H    -6.873890    -5.466745    -0.531774
 H    -8.620131    -9.681027    -1.206120
 H    -9.641680    -9.064578    -2.541898
 H   -10.379676    -9.520261    -0.975258
 H    -7.540729     3.262147     1.877378
 H    -8.727134     4.499867     2.254463
 H    -8.958730     5.017087    -0.208030
 H    -7.737069     3.800177    -0.568583
```

H	-6.054306	5.081670	0.792519
H	-7.278381	6.282266	1.185283
H	-7.510010	6.844672	-1.255154
H	-6.276574	5.653843	-1.646773
H	-4.605353	6.926445	-0.266024
H	-5.840020	8.109976	0.141808
H	-6.079782	8.699051	-2.292896
H	-4.840666	7.520003	-2.700215
H	-3.175241	8.789336	-1.309554
H	-4.414264	9.964689	-0.896594
H	-2.977029	10.824317	-2.759360
H	-4.636474	10.596587	-3.335147
H	-3.386098	9.414675	-3.750570
O	-8.885425	-1.712630	-3.980364
O	-5.738323	-1.945641	-2.114022
O	-5.218748	-2.301244	1.479762
O	-7.770899	-2.563005	4.135692
O	-11.516706	-2.547778	3.855591
O	-13.587628	-2.228264	0.888393
O	-12.346241	-1.886471	-2.618251
O	-8.815509	-7.820270	-4.553940
O	-5.611778	-8.026369	-2.850060
O	-5.254006	-8.365996	0.777560
O	-7.822975	-8.670261	3.489230
O	-11.493906	-8.661925	3.268457
O	-13.454142	-8.299406	0.224095
O	-12.323689	-7.977953	-3.206755
N	-7.700896	-3.463545	-4.950290
N	-5.581999	-3.594627	-3.746072
N	-4.343559	-3.793355	-1.893803
N	-4.006495	-4.033865	0.512057
N	-4.731803	-4.272342	2.612828
N	-6.417965	-4.440027	4.373430
N	-8.518122	-4.526163	5.135676
N	-10.952786	-4.513943	4.960976
N	-12.922539	-4.401109	3.905976
N	-14.305536	-4.193111	1.899747
N	-14.563231	-3.966100	-0.309638
N	-13.739578	-3.749995	-2.599270
N	-12.209942	-3.564484	-4.221942
N	-9.931801	-3.463528	-5.098048
N	-12.179922	-6.009785	-4.438502
N	-9.903556	-5.909321	-5.315615
N	-7.669959	-5.904797	-5.205667
N	-5.521117	-6.035858	-4.047321
N	-4.292604	-6.229176	-2.190800
N	-4.024539	-6.469645	0.225347
N	-4.743416	-6.711415	2.329891
N	-6.459675	-6.874453	4.061206
N	-8.525109	-6.972744	4.915573
N	-10.963028	-6.962531	4.763893
N	-12.894264	-6.843638	3.645423
N	-14.260334	-6.635655	1.634034
N	-14.542717	-6.406607	-0.571619
N	-13.770371	-6.187715	-2.878291
C	-8.844205	-2.769042	-4.595811
C	-6.375615	-2.916760	-4.751126
C	-5.281737	-3.000719	-2.533109
C	-3.644830	-3.343229	-0.707394
C	-4.717936	-3.418518	1.525213
C	-5.183601	-3.836783	3.919370
C	-7.592988	-3.718925	4.495644
C	-9.774524	-4.004132	5.632148
C	-11.764607	-3.697654	4.191846
C	-14.065644	-3.781019	3.269051
C	-14.086760	-3.346659	0.830173
C	-14.652534	-3.274047	-1.579626
C	-12.715268	-2.954582	-3.087589

C	-11.266087	-2.901368	-5.098002
C	-9.541743	-4.620954	-5.880457
C	-7.981021	-4.613050	-5.789307
C	-4.787338	-4.782750	-4.000190
C	-3.922057	-4.921342	-2.702849
C	-3.462069	-5.318598	0.908573
C	-3.968066	-5.485266	2.379955
C	-6.499240	-5.752178	4.983328
C	-7.955844	-5.799784	5.549576
C	-11.591099	-5.772018	5.304246
C	-12.955986	-5.704060	4.542698
C	-15.016129	-5.401314	1.519984
C	-15.206058	-5.237163	-0.025689
C	-14.020766	-4.884509	-3.461616
C	-12.929536	-4.772154	-4.576240
C	-11.227593	-6.485680	-5.420984
C	-8.799697	-6.666690	-4.966532
C	-6.335984	-6.467868	-5.164746
C	-5.194396	-6.883814	-3.008217
C	-3.618916	-6.899852	-1.097840
C	-4.739922	-7.295676	1.077158
C	-5.234157	-7.406902	3.501982
C	-7.629690	-7.616369	4.079806
C	-9.776828	-7.578587	5.319552
C	-11.748661	-7.600534	3.821171
C	-14.021412	-7.332317	2.881824
C	-14.016978	-7.225782	0.409747
C	-14.663715	-6.843616	-1.947811
C	-12.709021	-6.844846	-3.471824
H	-5.832814	-2.939330	-5.703700
H	-6.500141	-1.884210	-4.424243
H	-2.566271	-3.452420	-0.869278
H	-3.889957	-2.290413	-0.566047
H	-5.353645	-2.761611	3.859333
H	-4.395362	-4.045407	4.652875
H	-9.853355	-4.226443	6.703816
H	-9.757712	-2.924427	5.481966
H	-13.883562	-2.706294	3.252430
H	-14.961506	-3.993791	3.863804
H	-15.679732	-3.349781	-1.956522
H	-14.409929	-2.227905	-1.391632
H	-11.660632	-2.921643	-6.121203
H	-11.179907	-1.869219	-4.757887
H	-9.922735	-4.534965	-6.904635
H	-7.484307	-4.506715	-6.760600
H	-4.194604	-4.656056	-4.912982
H	-2.842934	-4.876897	-2.888022
H	-2.370143	-5.316170	0.815981
H	-3.160585	-5.574219	3.115662
H	-5.725144	-5.864512	5.751655
H	-8.000379	-5.897432	6.640509
H	-11.699346	-5.859892	6.391525
H	-13.829541	-5.783497	5.199950
H	-15.958638	-5.478683	2.073634
H	-16.255698	-5.212384	-0.339283
H	-15.046734	-4.827905	-3.842994
H	-13.342908	-4.689017	-5.587846
H	-11.125841	-7.561785	-5.279114
H	-11.622972	-6.283374	-6.424131
H	-6.442305	-7.549681	-5.083341
H	-5.818556	-6.216879	-6.098169
H	-2.537068	-6.756361	-1.202507
H	-3.855935	-7.960732	-1.180531
H	-4.453508	-7.393032	4.272548
H	-5.436821	-8.435860	3.204057
H	-9.761433	-8.613578	4.977412
H	-9.842968	-7.552972	6.413785
H	-13.815040	-8.374112	2.635585

```
 H   -14.926496    -7.272099     3.497736
 H   -14.426733    -7.907426    -1.970660
 H   -15.697426    -6.687470    -2.277521
```

LFD-01@CB[7] 1:1 complex, octyl side

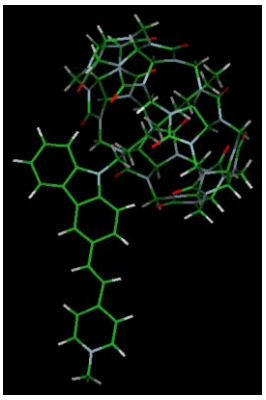

```
  189
scf done: -5408.665190
 N    -1.880141     0.833080     1.236339
 C    -3.275407     0.829890     1.198527
 C    -2.539872    -1.238251     0.524616
 C    -1.425575    -0.399688     0.825647
 C    -2.321358    -2.541281     0.090765
 C    -1.005743    -3.029850    -0.048861
 C     0.083323    -2.165076     0.260361
 C    -0.104899    -0.864211     0.691091
 C    -5.530195     1.586273     1.398078
 C    -5.996800     0.328087     0.975068
 C    -5.102011    -0.691712     0.657542
 C    -3.728065    -0.444705     0.766159
 C    -4.167825     1.858458     1.516927
 C    -0.825662    -4.388800    -0.511723
 C     0.349741    -5.053024    -0.695638
 C     0.478062    -6.409093    -1.168525
 C    -0.606582    -7.244630    -1.536363
 C    -0.388057    -8.526261    -1.980050
 N     0.866563    -9.037904    -2.083312
 C     1.934120    -8.270518    -1.740557
 C     1.768840    -6.982961    -1.292527
 C     1.080432   -10.428859    -2.528609
 C    -1.051948     1.985251     1.588378
 C    -0.813373     2.946798     0.414251
 C     0.032135     4.152511     0.844155
 C     0.242862     5.187298    -0.267859
 C     1.106035     6.375553     0.177256
 C     1.298682     7.442164    -0.907040
 C     2.174572     8.618249    -0.453485
 C     2.348152     9.685885    -1.538995
 H    -3.160882    -3.190546    -0.145438
 H     1.100183    -2.527404     0.149404
 H     0.747972    -0.226027     0.897194
 H    -6.243104     2.371384     1.634104
 H    -7.065605     0.152126     0.893517
 H    -5.464590    -1.662325     0.329356
 H    -3.832581     2.839448     1.836525
 H    -1.755043    -4.912431    -0.729097
 H     1.289446    -4.553745    -0.476091
 H    -1.631230    -6.898959    -1.483373
 H    -1.198261    -9.183778    -2.268079
 H     2.908168    -8.732692    -1.842036
 H     2.650562    -6.407445    -1.034189
 H     1.888457   -10.450407    -3.260889
```

H	0.164757	-10.798727	-2.987127
H	1.340150	-11.050920	-1.669123
H	-0.099886	1.613605	1.975463
H	-1.540062	2.509803	2.416381
H	-1.779995	3.288883	0.020589
H	-0.314069	2.406653	-0.400825
H	1.009039	3.798168	1.202814
H	-0.449229	4.640580	1.703987
H	-0.735317	5.555844	-0.610974
H	0.709909	4.702566	-1.138178
H	2.090448	6.005311	0.500607
H	0.649857	6.840166	1.064366
H	0.316763	7.824634	-1.222897
H	1.750019	6.981607	-1.797991
H	3.159423	8.235843	-0.149934
H	1.732410	9.074101	0.443846
H	2.979386	10.513089	-1.193324
H	1.378998	10.105183	-1.836322
H	2.814202	9.262263	-2.437460
O	4.228221	6.196645	-3.345568
O	5.491598	6.380745	0.178041
O	4.012722	7.932182	3.169358
O	0.868297	9.697141	3.251018
O	-1.495088	10.261673	0.394657
O	-1.425626	9.348996	-3.223618
O	1.158625	7.500476	-4.927361
O	1.561992	0.823727	-2.093889
O	2.755529	1.018455	1.363599
O	1.076743	2.629699	4.263889
O	-2.173792	4.515901	4.373491
O	-4.665681	5.204197	1.818432
O	-4.294029	4.164860	-1.678713
O	-1.584538	2.234545	-3.391069
N	4.688744	4.009345	-2.701694
N	5.496615	4.128559	-0.403518
N	5.425166	4.679244	1.761739
N	4.349151	5.693659	3.702529
N	2.748640	6.826554	4.778043
N	0.643662	8.064609	4.891811
N	-1.199477	8.848180	3.897356
N	-2.772451	9.311739	2.090042
N	-3.514813	9.182702	-0.015431
N	-3.419143	8.516464	-2.360890
N	-2.541829	7.543115	-4.171553
N	-0.783692	6.279678	-5.306626
N	1.178952	5.209413	-5.328608
N	3.265845	4.355237	-4.391023
N	0.071764	3.086708	-4.783663
N	2.157313	2.234376	-3.843166
N	3.652369	1.834151	-2.229173
N	4.452540	1.956459	0.077731
N	4.265343	2.563512	2.221989
N	3.201106	3.573054	4.173916
N	1.560023	4.712077	5.176823
N	-0.545791	5.941253	5.231569
N	-2.458347	6.820950	4.476891
N	-4.023797	7.276466	2.655673
N	-4.773411	7.152090	0.553661
N	-4.635528	6.462300	-1.785992
N	-3.629422	5.444449	-3.504066
N	-1.870449	4.183058	-4.627749
C	4.067915	4.988027	-3.458653
C	5.786795	4.316545	-1.809724
C	5.460204	5.194358	0.478957
C	5.563957	5.515517	2.934678
C	3.726104	6.925629	3.803241
C	2.038645	7.989235	5.271025
C	0.182110	8.943050	3.928788

C	-2.008235	9.830728	3.203798
C	-2.478250	9.641711	0.778947
C	-3.645669	9.577747	-1.402853
C	-2.352492	8.549086	-3.242111
C	-1.698221	7.401289	-5.339677
C	0.580514	6.444740	-5.149033
C	2.614617	5.073119	-5.465986
C	3.352779	2.910532	-4.316462
C	4.382882	2.667296	-3.164754
C	5.581286	2.846685	0.274427
C	5.480792	3.231930	1.786521
C	3.876624	4.746358	4.695758
C	2.734885	5.528759	5.425672
C	-0.425936	7.353777	5.560910
C	-1.718220	7.976244	4.939859
C	-4.061928	8.663584	2.229393
C	-4.583172	8.576634	0.757234
C	-4.424427	7.536399	-2.736000
C	-3.777636	6.814871	-3.964473
C	-1.148247	4.919830	-5.651130
C	0.229431	4.181709	-5.719907
C	0.994065	1.978125	-4.668000
C	2.364470	1.560320	-2.652791
C	4.259121	1.147204	-1.108308
C	3.711522	1.773548	1.230216
C	3.880359	2.424793	3.612960
C	1.857127	3.543495	4.499493
C	0.282577	4.910907	5.826222
C	-1.765710	5.637441	4.649887
C	-3.834786	6.858059	4.029747
C	-4.493020	6.409442	1.685539
C	-5.447652	6.579963	-0.593091
C	-4.185855	5.240568	-2.253350
C	-3.287631	4.338765	-4.374343
C	-1.168322	3.081334	-4.170735
H	6.650539	3.697256	-2.082234
H	6.032514	5.369500	-1.949606
H	6.337793	5.086451	3.582596
H	5.876521	6.503057	2.594478
H	2.532886	8.867298	4.854890
H	2.106524	8.009878	6.364675
H	-2.698990	10.294675	3.918768
H	-1.328203	10.585633	2.808497
H	-2.894974	10.345233	-1.592907
H	-4.647494	9.996571	-1.559194
H	-2.337794	7.310036	-6.225223
H	-1.094130	8.305807	-5.412818
H	2.837613	4.564542	-6.411808
H	3.031075	6.080534	-5.484193
H	3.667827	2.497096	-5.281486
H	5.297419	2.159841	-3.492790
H	6.515972	2.337654	0.012632
H	6.334890	2.893738	2.384399
H	4.697218	4.449281	5.359104
H	2.899632	5.639699	6.503564
H	-0.351475	7.486319	6.646438
H	-2.316339	8.551133	5.655914
H	-4.712320	9.246215	2.892076
H	-5.523970	9.114479	0.592185
H	-5.374347	8.031694	-2.967658
H	-4.395008	6.848212	-4.869414
H	-1.704928	4.902720	-6.595178
H	0.473080	3.797347	-6.717157
H	0.452022	1.152272	-4.206690
H	1.323115	1.687016	-5.672882
H	3.596577	0.325807	-0.835341
H	5.230863	0.748317	-1.423024
H	4.774987	2.213130	4.211362

H	3.192268	1.581409	3.673050
H	0.450721	5.151780	6.883356
H	-0.265674	3.971704	5.748708
H	-4.231463	5.846189	4.113619
H	-4.397123	7.531300	4.687952
H	-5.758058	5.573742	-0.310865
H	-6.330255	7.186417	-0.828188
H	-3.630919	3.426211	-3.886306
H	-3.809324	4.463284	-5.331498

Table S4. Results of BSSE calculations and complexation energies:

	Pyridinium complex	Octyl complex	Δ / kcal.mol^{-1}
BSSE / (vacuum)	0.014217 ha	0.015769 ha	0.97
In vacuum			
Energy	-5408.5245 ha	-5408.4971 ha	-17.19 **(pyridinium)**
Complexation Energy	-45.81 kcal.mol^{-1}	-28.61 kcal.mol^{-1}	-17.20 **(pyridinium)**
Corrected Complexation Energy	-36.89 kcal.mol^{-1}	-18.72 kcal.mol^{-1}	-18.17 **(pyridinium)**
In water			
Energy	-5408.6672 ha	-5408.6652 ha	-1.26 **(pyridinium)**
Complexation Energy	-11.17 kcal.mol^{-1}	-9.91 kcal.mol^{-1}	-1.26 **(pyridinium)**
Corrected Complexation Energy	-2.25 kcal.mol^{-1}	-0.02 kcal.mol^{-1}	-2.23 **(pyridinium)**

Complexation Energy = $E_{complex} - (E_{CB7} + E_{guest})$.
Corrected Complexation Energy = $E_{complex} - (E_{CB7} + E_{guest})$ + BSSE.

$E_{CB7(water)}$ = -4212.3881 ha.
$E_{CB7\ (vacuum)}$ = -4212.2516 ha.
$E_{guest\ (water)}$ = -1196.2613 ha.
$E_{guest\ (vacuum)}$ = -1196.1999 ha.

Supplementary References

[1] Liu, Y. *et al.* A water-soluble and fast-response mitochondria-targeted fluorescent probe for colorimetric and ratiometric sensing of endogenously generated SO_2 derivatives in living cells. *Chem. Commun.* **52,** 3430-3433 (2016).

[2] Dey, G., Gaur, P., Giri, R. & Ghosh, S. Optical signaling in biofluids: A nondenaturing photostable molecular probe for serum albumins. *Chem. Commun.* **52,** 1887-1890 (2016).

[3] Zaman, M. B. *et al.* Size reduction of CdSe/ZnS quantum dots by a peptidic amyloid supergelator. *ACS Appl. Mater. Interfaces* **4,** 1178-1181 (2012).

[4] Bardelang, D. *et al.* Cucurbit[n]urils (n = 5–8): A comprehensive solid state study. *Cryst. Growth Des.* **11,** 5598-5614 (2011).

[5] Zhang, K.-D.; Ajami, D.; Rebek, J. Hydrogen-bonded capsules in water. *J. Am. Chem. Soc.* **135**, 18064-18066 (2013).

[6] Lee, B. & Richards, F. M. The interpretation of protein structures: Estimation of static accessibility. *J. Mol. Biol.* **55,** 379-IN374 (1971).

[7] Cossi, M., Rega, N., Scalmani, G. & Barone, V. Energies, structures, and electronic properties of molecules in solution with the c-pcm solvation model. *J. Comput. Chem.* **24,** 669-681 (2003).

[8] Breneman, C. M. & Wiberg, K. B. Determining atom-centered monopoles from molecular electrostatic potentials. The need for high sampling density in formamide conformational analysis. *J. Comput. Chem.* **11,** 361-373 (1990).

[9] Frisch, M. J.; Trucks, G. W.; Schlegel, H. B.; Scuseria, G. E.; Robb, M. A.; Cheeseman, J. R.; Scalmani, G.; Barone, V.; Mennucci, B.; Petersson, G. A.; Nakatsuji, H.; Caricato, M.; Li, X.; Hratchian, H. P.; Izmaylov, A. F.; Bloino, J.; Zheng, G.; Sonnenberg, J. L.; Hada, M.; Ehara, M.; Toyota, K.; Fukuda, R.; Hasegawa, J.; Ishida, M.; Nakajima, T.; Honda, Y.; Kitao, O.; Nakai, H.; Vreven, T.; Montgomery, Jr., J. A.; Peralta, J. E.; Ogliaro, F.; Bearpark, M.; Heyd, J. J.; Brothers, E.; Kudin, K. N.; Staroverov, V. N.; Kobayashi, R.; Normand, J.; Raghavachari, K.; Rendell, A.; Burant, J. C.; Iyengar, S. S.; Tomasi, J.; Cossi, M.; Rega, N.; Millam, J. M.; Klene, M.; Knox, J. E.; Cross, J. B.; Bakken, V.; Adamo, C.; Jaramillo, J.; Gomperts, R.; Stratmann, R. E.; Yazyev, O.; Austin, A. J.; Cammi, R.; Pomelli, C.; Ochterski, J. W.; Martin, R. L.; Morokuma, K.; Zakrzewski, V. G.; Voth, G. A.; Salvador, P.; Dannenberg, J. J.; Dapprich, S.; Daniels, A. D.; Farkas, Ö.; Foresman, J. B.; Ortiz, J. V.; Cioslowski, J.; Fox, D. J. . Gaussian 09, revision d.01. Gaussian, Inc. (2009).

[10] Dumur, F., Mayer, C. R., Dumas, E., Miomandre, F., Frigoli, M. & Sécheresse, F. New chelating stilbazonium-like dyes from michler's ketone. *Org. Lett.* **10,** 321-324 (2008).

[11] Dumur, F. *et al.* Electrochemical, linear optical, and nonlinear optical properties and interpretation by density functional theory calculations of (4-n,n-dimethylaminostyryl)-pyridinium pendant group associated with polypyridinic ligands and respective multifunctional metal complexes (RuII or ZnII). *Inorg. Chem.* **48,** 8120-8133 (2009).

[12] Tehfe, M.-A. *et al.* New pyridinium salts as versatile compounds for dye sensitized photopolymerization. *Eur. Polym. J.* **49,** 567-574 (2013).

[13] Handelman, A., Kuritz, N., Natan, A. & Rosenman, G. Reconstructive phase transition in ultrashort peptide nanostructures and induced visible photoluminescence. *Langmuir* **32,** 2847-2862 (2016).

[14] Johnson, E. K., Adams, D. J. & Cameron, P. J. Directed Self-Assembly of Dipeptides to Form Ultrathin Hydrogel Membranes. *J. Am. Chem. Soc.* **132,** 5130−5136 (2010).